Final Report

RI 97-019

SIGNAL MAST ARM FATIGUE FAILURE INVESTIGATION

MISSOURI DEPARTMENT OF TRANSPORTATION
RESEARCH, DEVELOPMENT AND TECHNOLOGY

By: Genda Chen, Ph.D., P.E.
M. Barker, Ph.D., P.E.
L. R. Dharani, Ph.D.
C. Ramsay, Ph.D.

Acknowledgment to:

University Transportation Center at the University of Missouri-Rolla

JEFFERSON CITY, MISSOURI
DATE SUBMITTED: May 30, 2003

The opinions, findings, and conclusions expressed in this publication are those of the principal investigators and the Missouri Department of Transportation. They are not necessarily those of the U.S. Department of Transportation, Federal Highway Administration. This report does not constitute a standard, specification or regulation.

ACKNOWLEDGEMENTS

The authors would like to express their deep appreciation to continuing coordination provided by Vince Imhoff, P.E., and Tom Allen, P.E. from the Missouri Department of Transportation. Special thanks are due to several graduate students for their significant contributions to the research project. They include Jingning Wu, Ph.D. candidate, Jiaqing Yu, Ph.D. Candidate, Scott MacKenzie, Ph.D. Candidate, and Joseph L. Alderson, Master student.

EXECUTIVE SUMMARY

The Missouri Department of Transportation (MoDOT) has discovered and documented failures in several cantilever mast arms in the recent years. The failures were primarily by fatigue at the weld of the arm to the base plate attached to the mast. With over 6000 mast arms in service in Missouri, the failures raised concerns with the existing mast arm inventory and future mast arm design.

This report presents findings from an effort to determine the cause of unexpected cracking in Missouri mast arms. Three causes of premature failure were investigated: the stress ranges experienced at the weld detail were higher than anticipated, the number of cycles experienced at the weld detail were larger than anticipated and/or the weld quality and, therefore, fatigue resistance of the weld detail was less than expected. The endeavor was a collaboration between the University of Missouri-Rolla and the University of Missouri-Columbia

Two mast arms were instrumented in the field to determine the stresses experienced by the arms and to develop wind load models for Missouri. Five mast arms were fatigue tested in the laboratory, some with a proposed "fatigue-resistant" weld detail. Failed mast arms from in service and the laboratory were metallurgically examined to determine the failure mechanisms and evaluate weld quality. Fatigue resistant strength and remaining life predictions were developed from the experimental results and theoretical fracture mechanics.

The results show that the main culprit for the premature fatigue failure of mast arms in Missouri can be attributed to poor weld quality. The new "fatigue-resistant" weld detail, without quality welding techniques, does not improve the situation. The loads and cycles of loads experienced by the mast arms are not necessarily critical if the weld is of high quality. Recommendations for possible solutions for existing in-service mast arms and for new mast arms are presented. The recommendations range from insuring weld quality to dampers on the mast arms.

TABLE OF CONTENTS

Page

LIST OF TABLES

Page

LIST OF FIGURES

Page

LIST OF SYMBOLS

The following symbols have been used in the report:

A_c, A_1, A_2, A_3, A_4 = cross sectional area

B(x) = diameter

C_D, C_L = wind drag and lift coefficients

F_{G1}, F_{G2}, F_{G3}, F_{G4}, $F_{NW,}$ F_{TG} = wind load

I_c = moment of inertia

I_F = importance factor

m(x) = mass per unit length

M_y, M_z = bending moment

$P_{G,}$ $P_{NW,}$ P_{TG} = wind pressure

R_c = radius

Re = Reynolds number

S_c = section modulus

U, U_g = wind speed

Y_1 = generalized coordinate of the 1st mode

α = attack angle of the wind

ξ = damping ratio

ρ = mass density of air

ρ_s = mass density of steel

σ, σ_c = normal stress

υ = wind speed

$\phi_1(x)$ = vibration shape of the 1st mode

ω_1 = fundamental frequency

1. INTRODUCTION

1.1 Problem Statement

The Missouri Department of Transportation (MoDOT) has discovered and documented failures in several cantilever mast arms in the recent years. The failures were primarily by fatigue at the weld of the arm to the base plate attached to the mast. Most of the failures involved octagon shaped arms manufactured by JEM, Inc. Other mast arms that have failed were produced by Union Metals and Valmont. With over 6000 mast arms in service in Missouri, the failures raised concerns with the existing mast arm inventory and future mast arm design.

1.2 Background and Objectives

This report is the result of the efforts of the University of Missouri-Columbia (UMC) and the University of Missouri-Rolla (UMR) to examine the problem of mast arm fatigue cracking in Missouri. Unexpected fatigue failures can be precipitated from several sources. The sources could be that the stress ranges experienced at the weld detail were higher than anticipated, the number of cycles experienced at the weld detail were larger than anticipated and/or the weld quality and, therefore, fatigue resistance of the weld detail was less than expected. These issues were investigated by the UMC/UMR collaborative research project.

UMC was responsible for instrumenting two mast arms in the field and collecting in service stress data. UMC also fatigue tested five full-scale mast arms from the three manufacturers with various weld details. UMR examined the metallurgical failure mechanism of several failed mast arms (from the field and the laboratory tested failures) and the weld quality issues. UMR also developed fatigue loading, resistance and life prediction models for Missouri mast arms.

With these tasks, the stress range, number of cycles and weld quality issues thought responsible for failure were examined and conclusions derived to address the failure of mast arms in Missouri. Chapter 6 presents the findings and conclusions from the research.

1.3 Organization of Report and Research Description

Chapter 2 examines the metallurgical analyses of the failed mast arms and the weld quality issues. Full-scale fatigue test results are also presented. Of the five laboratory tests, three failed well prior to expected from fatigue design predictions. Also, the "fatigue-resistant" weld detail did not seem to improve the fatigue resistance. The chapter concludes that the most significant finding of this work is that there are problems with weld quality in the mast arms as manufactured. Although there was a definite lack of fusion at the root of the weld, the most detrimental characteristics were that there was significant undercutting and sharp features leading to high stress concentrations and premature cracking. The new "fatigue-resistant" weld proposed to increase fatigue strength fared no better and still has the undercutting and sharp feature problems. Thus, weld quality was determined to be the main culprit in the unexpected fatigue failure of Missouri mast arms.

Chapter 3 investigates the proposed (3rd Draft) AASHTO *Standard Specifications for Structural Supports for Highway Signs, Luminaries and Traffic Signals* (1999). These specs were developed in NCHRP Report 412 (Kaczinski et al, 1998). Equivalent static loads were developed for the four types of dynamic loading: galloping, vortex shedding, natural wind gusts and truck induced gusts. Stress ranges produced are compared to the constant amplitude fatigue limit (CAFL) for the appropriate connection detail. Importance factors are introduced to adjust

the level of reliability of cantilevered mast arms to account for the "importance" of the mast arm. The results show that, if the new specs are used, the size of mast arms would greatly increase, even at the lowest importance category. The consequence of such action would be a significant increase in cost and space of new mast arms. However, the draft spec does give a clear and consistent design process for fatigue in mast arms.

Chapter 4 studies the in-service loading of mast arms in Missouri. Two in-service mast arms, Stadium & Forum and Providence & Green Meadows, were instrumented in the field. The field test data from mast arms were used with National Climatic Data Center data to develop wind distribution models. Truck-induced wind and galloping models were also developed. The results included number of cycle predictions for Missouri mast arms. These models were used in Chapter 6 to develop life-prediction models for in-service and new mast arms.

Chapter 5 deals with the stress analysis of weld joint areas using finite element techniques and the determination of stress concentration and stress intensity factors needed in the fatigue life and propagation life predictions, respectively. The influence of weld quality on the predicted remaining life of mast arms is presented. The results show that, if the weld is of high quality, there should not be fatigue problems with the Stadium & Forum or the Providence & Green Meadows mast arms for their remaining life. However, with lower weld quality, as seems the case, the Stadium & Forum mast arm is susceptible to fatigue cracking (mainly due to its length).

1.4 Summary

Chapter 6 presents the overall findings and conclusions of this research. Clearly the main culprit for the premature fatigue failure of mast arms in Missouri can be attributed to poor weld quality. The new "fatigue-resistant" weld detail, without quality welding techniques, does not improve the situation. The loads and cycles of loads experienced by the mast arms are not necessarily critical if the weld is of high quality.

Reducing or eliminating weld fatigue failures can be achieved by either increasing the fatigue resistance of the weld detail or reducing the stress range and/or number of cycles. Chapter 6 presents recommendations for possible solutions for existing in-service mast arms and for new mast arms. The recommendations range from insuring weld quality to dampers on the mast arms.

2. CAUSE OF FAILURES IN MAST ARMS

This section addresses the failure analysis of one in-service mast arm and another arm tested to failure in laboratory. Both arms were observed to fail by fatigue. Crack initiated at the toe of the weld in each. In addition, laboratory tests were conducted on five prototype arms to investigate the effect of the new weld profile on fatigue strength and to compare the fatigue performance of mast arms supplied by various manufacturers.

2.1 Joint and Weld Details

In Missouri, traffic sign and signal-support structures are typically constructed with cold-form steel. They are cantilevered structures consisting of a vertical post and a horizontal mast arm. The post is typically octagonal in shape and a solid steel plate is welded on the side of the post for connection with the horizontal arm as shown in Figure 2.1. The mast arm comes with either circular or octagonal shapes. It is attached to a base plate with two fillet weldments around its circumference. The first weld is on the outside and would be visible when the mast arm assembly is in service as pointed out in Figure 2.1. The second weld is at the end of the arm and on the inside of the hole on the base plate that was cut to mate the octagonal shape of the arm. A schematic diagram showing a cross sectional view of the mast arm assembly and the locations of the two weldments are presented in Figure 2.2. Note that the end of the arm is not flushed with the surface of the base plate. The post and arm are individually pre-fabricated in the factory. They are assembled together in the field with four bolts as observed in Figure 2.1.

The cracks on all failed mast arms are located at the connection of arm to the base plate. They were observed to initiate on top of the arms and are primarily associated with the bending effect of the mast arms in the vertical plane.

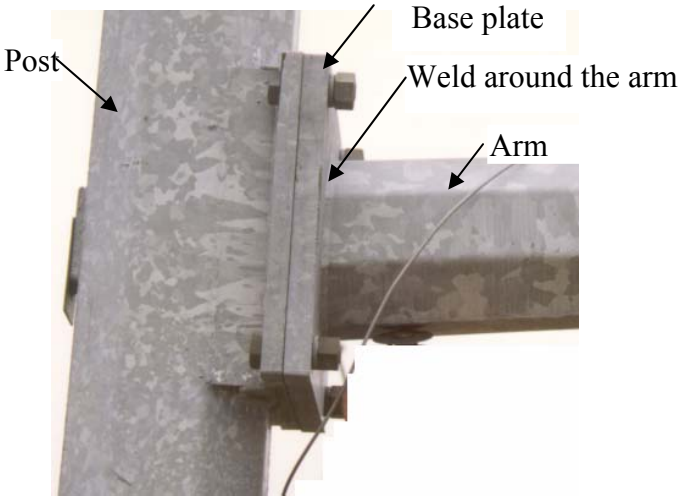

Figure 2.1 Arm-to-post connection

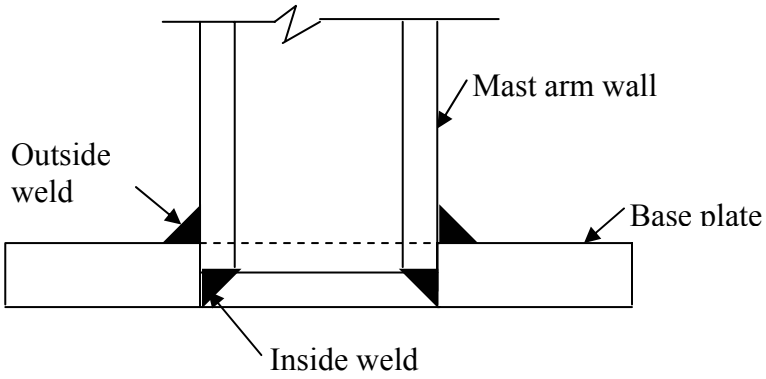

Figure 2.2 Cross sectional view of a mast arm and base plate

2.2 Failure of In-Service Mast Arms

Multiple cantilevered signal mast arms have been reported to have failed in the St. Louis region (Bennett, 1997). Of a known 10 failures, 60% have been manufactured by JEM, Inc. Excluding the mast arms that have lasted longer than 20 years, the proportion of failed mast arms manufactured by JEM increases to 75%. In each of the failures (except a failure that had two arms), cracking initiated near a weld that connects the mast arm to the connection plate. The mode of cracking was reported to be by fatigue.

Using ultrasonic inspection, additional 35 arms were found to contain a flaw. However, no details regarding the technique used was provided and no inspection criteria were provided. In fact, no detection thresholds exist for this weld configuration. An independent testing laboratory, St. Louis Testing, examined the weld of a new replacement signal mast arm section from JEM. This weldment was examined by ultrasonic testing and by a metallographic section through the weld (Hillner, 1997). The laboratory also cited the existence of an ultrasonic indication. However, they could not interpret the results because of the lack of inspection criteria. The metallographic section showed non-fusion and poor penetration of the weld metal.

On the basis of these findings, a series of design recommendations were made (Porter, 1996) to the Signal Mast Arm Standard Drawing (MHTD 902.40). These recommendations included:

(1) A decrease in the permissible stresses from140% to 133% of the allowable stresses (dead load + wind load or dead load + ice load + 0.5 wind load);

(2) The minimum wind design speed was increased to from 80 mph to 90 mph;

(3) The use of AWS D1.1-96 Structural Welding Code;

(4) Magnetic particle inspection of the weldments;

(5) and the use of a more fatigue resistant weld profile.

2.2.1 Investigation

One failed octagonal mast arm was studied for the causes of its fracture. The arm and the fracture surface were first examined visually. Four sample specimens were then prepared and, both metallurgical and fractographic analyses were conducted to determine the reason for their cracking.

2.2.1.1 Visual Examination of the Failed Mast Arm

The mast arm examined is shown in Figure 2.3. It consists of two weldments, one at the end of the tube and one on the exterior surface of the tube. Each of the weldments is a fillet weld. The appearance of the weld bead indicates that welding was discontinuous, with each flat of the mast arm tube as an individual weld. There was some attempt to tie-in the welds on the other flats. The progression of the weld solidification pattern indicates that welding was performed in a single direction. The weld on each flat ended at the corner of the flats. There appeared to be no evidence of "buttering back" to prevent crater cracks. At the toe of the weld, undercutting was apparent on both the signal mast arm and on the base plate as evidenced in Figure 2.4. It appeared to be more severe on the side of the mast arm. The shape of the weld bead was convex in relation to the fillet.

2.2.1.2 Visual Examination of the Fracture Surface of the Failed Arm

A cursory visual examination of a signal mast arm failure was also performed. The fracture showed lack of fusion in several places, and had the characteristic blue temper colors showing exposure to heat. Several locations on the fracture had a morphology that suggested fatigue that had initiated at multiple locations at the outer surface at the toe of the weld. Initiation and propagation of cracking was through the base metal. No beachmarks were observed. However, this is not unusual in weldments. No effort was made to confirm the presence of fatigue using the scanning electron microscope.

2.2.1.3 Procedure of Failure Analysis

For fractographic analysis, a fracture surface was opened on the mast arm for observation. This allows the determination of the crack initiation sites. This was accomplished by flame cutting the material approximately two inches ahead of the cracked portion of the weldment and then saw cutting to allow the fracture to be opened. The fractographic analysis was followed by the metallographic evaluation of the weld metal, base plate materials, and features of the weldment such as the heat zone, fusion line, grain refined region, and degree of penetration of the weldment.

2.2.1.4 Metallographic Examination of the Failed Arm

Four metallographic specimens were taken from a variety of locations in the mast arm assembly shown in Figure 2.2. Specifically, two specimens were cut from the outside weld in cracked and uncracked regions, which are respectively designated "CT: and "ET". The other two specimens were cut from the inside weld in cracked and uncracked regions, respectively denoted as "BC" and "BE". The metallographic sections were polished to remove any oxidation and were then etched using 2% Nital (2ml HNO_3, 98 ml CH_3OH). The resulting sections are shown in Figure 2.5.

Examination of these sections showed a lack of fusion in any of the metallographic sections. There is no evidence of any weld preparation. On the inside welds, the weld bead in Figures 2.6 and 2.7 showed a typical microstructure of acicular ferrite. The heat affected zone (HAZ) showed evidence of banded spherodized pearlite. The base material was also banded, and exhibited distinct regions of very fine pearlite. This structure is not unusual for A36 steel that has been hot rolled. The radius at the toe of the weld is sharp. A sharp undercut of the weld is also evident. The undercut is approximately 50 to 100 μm deep, and 200 μm wide. This is a very sharp notch, and occurs where the base material is the softest, and least resistant to fatigue.

In the outside weld (Specimen ET), the weld bead shown in Figure 2.8 at three locations presented evidence of undercutting at the site of crack initiation of the fracture surface. The close-up view at location C1 confirmed the cracking. The small size of the shear lip indicates that the stress levels were small in comparison to the overall section size. At the region of the root of the fillet, evidence of porosity, and cracks linking regions of porosity, was observed. This probably occurred by overload, possible during the final failure. This is indicated by the direction of cracking, perpendicular to the fracture. However, this could have also occurred because of residual stresses in the weld.

At the fillet of the weld opposite the primary fracture, a small secondary crack, approximately 125 μm long, was observed propagating parallel to the primary fracture. This crack was observed to be propagating from a region of undercut at the toe of the weld. The radius of the weld bead to the base material was also sharp. This indicates a substantial stress concentration. The straight nature of the crack is indicative of a fatigue crack. The presence of a small fatigue crack at the toe of the weld at the base plate, parallel to the primary fracture, shows that failure is not limited to crack initiation at the weld toe on the side of the signal mast arm.

2.2.2 Discussions

It is clear that the weld quality is poor. There is lack of fusion and lack of penetration. This can be improved by proper joint preparation and preheating the weld. Better penetration of the weld could be achieved by creating a small 45^{o} bevel at the edge of the base plate where the mast arm meets the base plate. This bevel could be readily achieved by grinding immediately prior to welding. This would improve the amount of weld fusion and penetration. It would also provide a concave weld bead shape that is more conducive to fatigue service. This would reduce the sharp radius produced by the convex weld shape, reducing the high stress concentration.

However, failure of the mast arm did not result from poor penetration or lack of fusion. Failure occurred in the base metal. Even these poor welds were adequate to hold the base plate and the mast arm together. Failure initiated at a region of undercutting at the toe of the weld. This was aggravated by the undercutting in the region of the heat affected zone, where the base metal is softest, and least able to resist fatigue. The presence of undercutting, and the resultant large stress concentration factor is likely the source of premature fatigue crack initiation. Undercutting at the toe of a weld bead is caused by several things, including excessive current, too long of an arc, too large of an electrode and the incorrect electrode angle. It is symptomatic of poor welding procedures or inexperienced welding operators.

Figure 2.3 Overview of the failed arm-to-plate connection

ı Figure2.4 View of the typical outer weld on the luminare stanchion

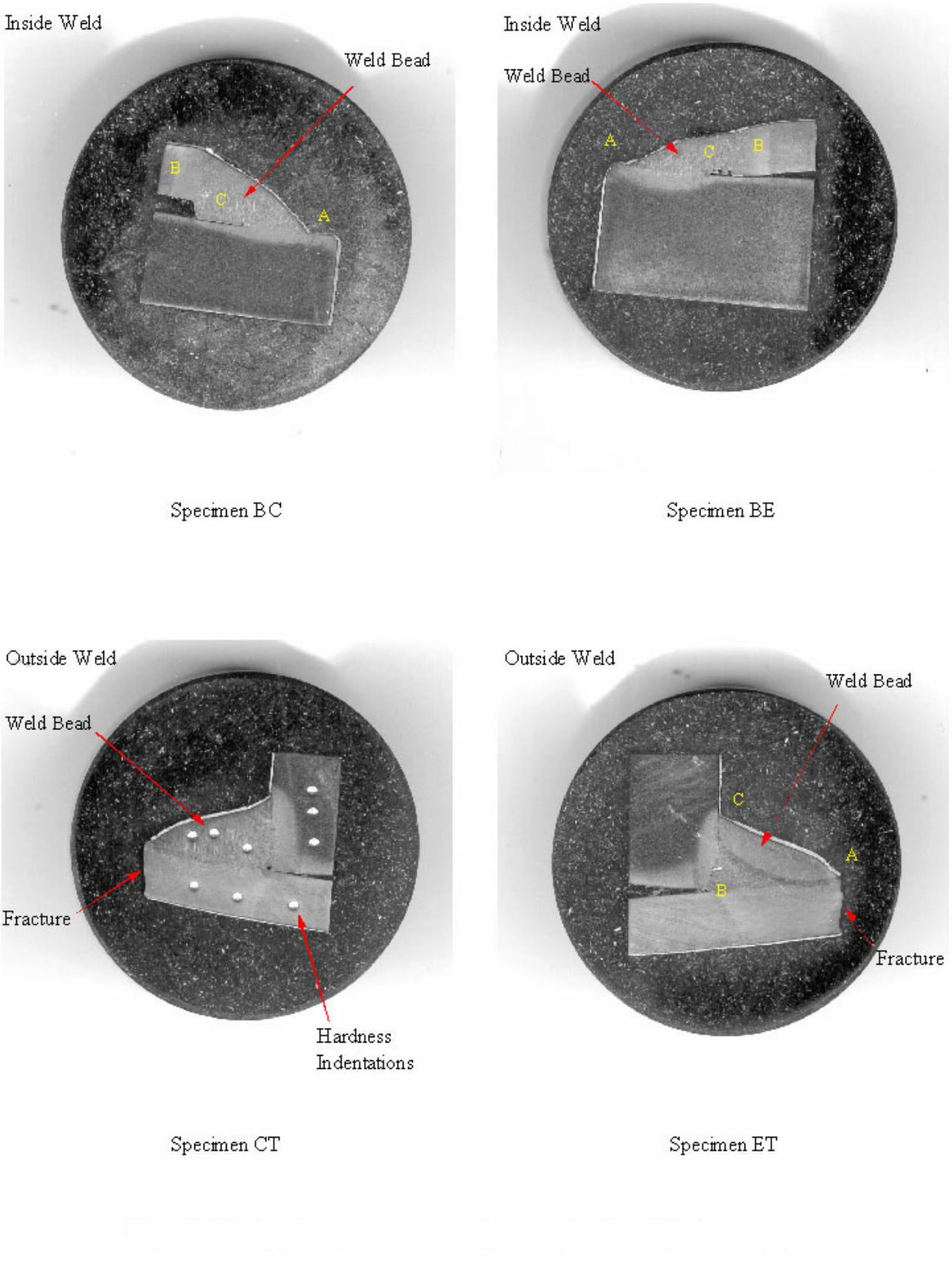

Figure 2.5 Metallographic specimens examined, showing locations of photomicrographs

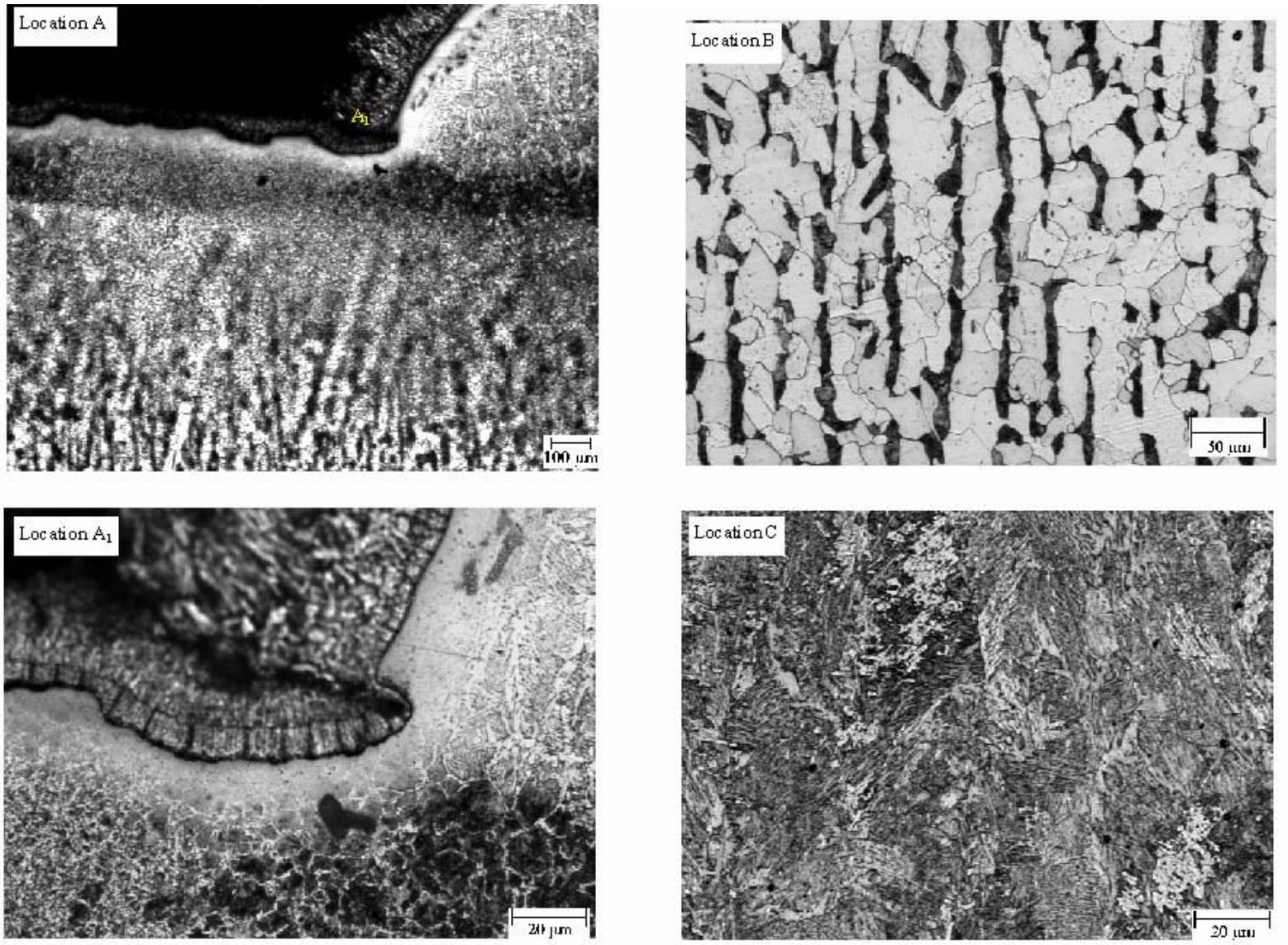

Figure 2.6 Selected photomicrographs from Specimen BC

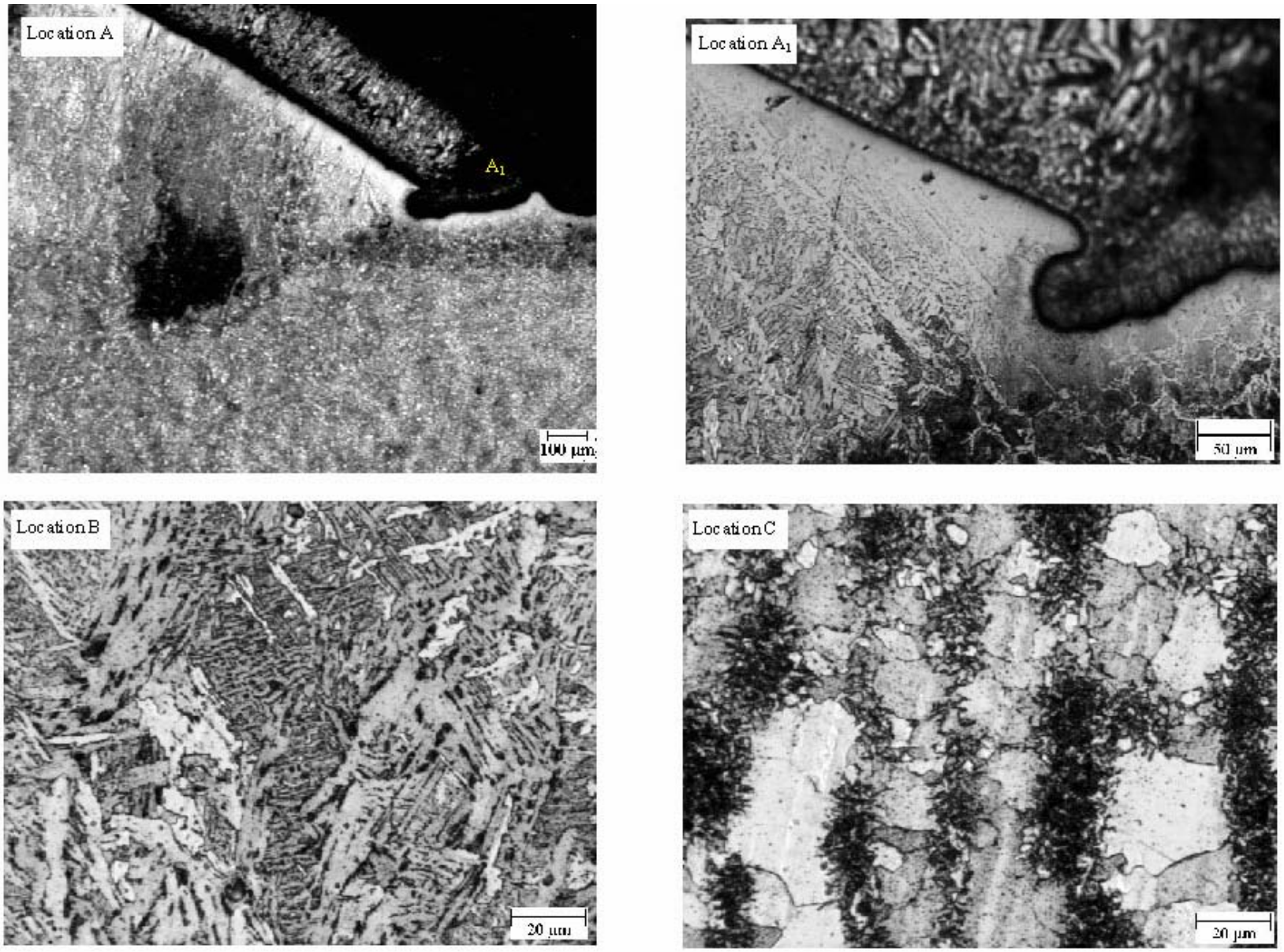

Figure 2.7 Selected photomicrographs from Specimen BE

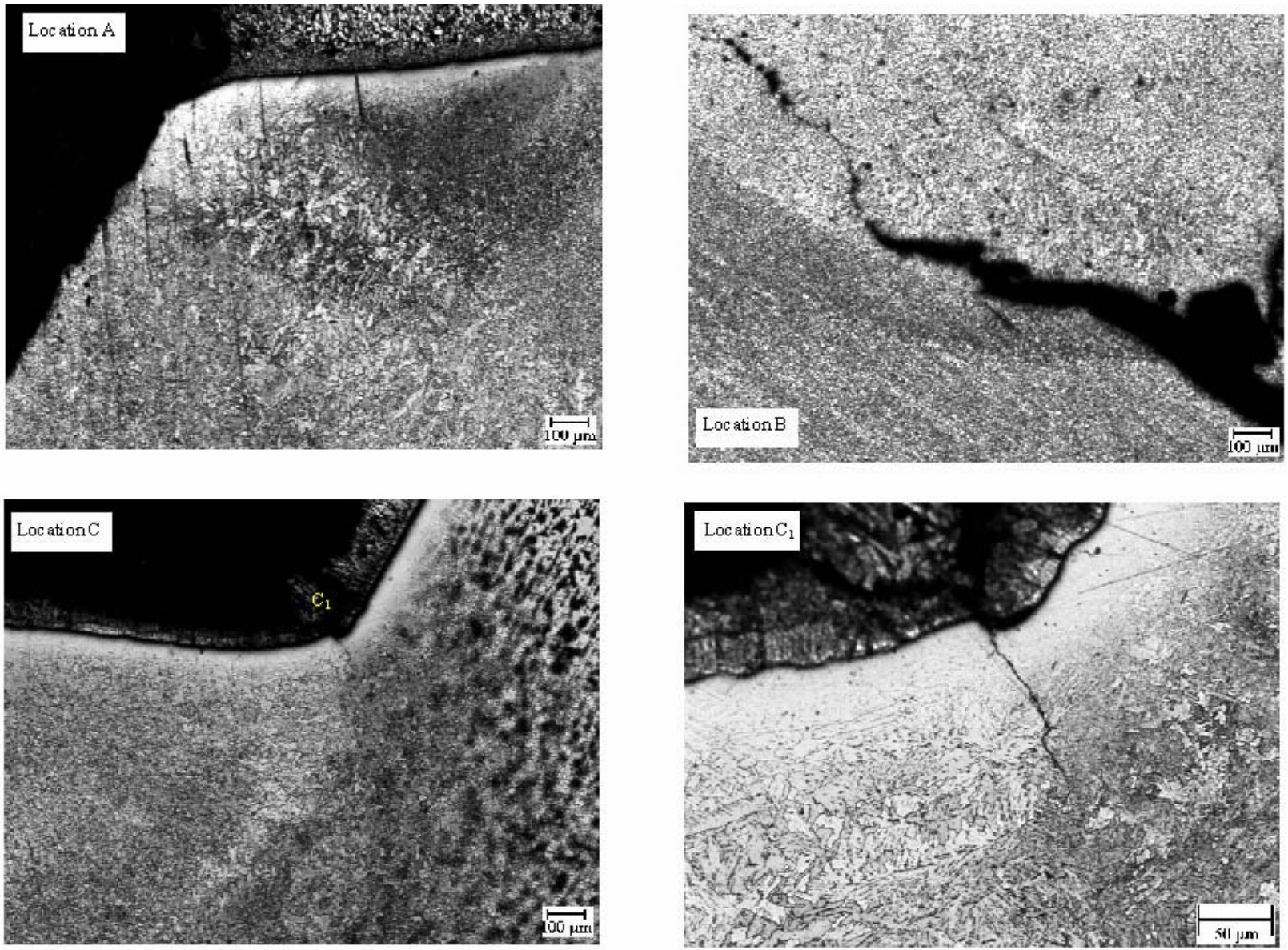

Figure2.8 Selected photomicrographs from Specimen ET

2.3 Failure of Laboratory Specimens

To determine the fatigue strength of a typical weld connection as shown in Figure 2.1, five full-scale arms were tested in the laboratory. They include products from three manufacturers and two with a new "fatigue-resistant" weld (Figure 2.9). The main objectives of these tests are two fold. One was to verify if the "fatigue-resistant" weld increases the fatigue strength and the other was to compare the performance of the mast arms from three vendors.

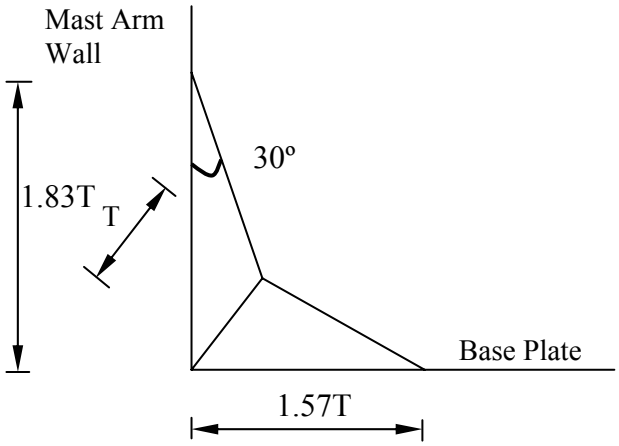

Figure 2.9 Fatigue-resistant weld

2.3.1 Laboratory Test Set up

Fatigue testing was performed on five full-scale mast arm specimens. A full description of the testing and results can be found in Alderson (1999). Herein is presented the overall testing procedures and results. The mast arms were connected to a stiffened backstop post, shown in Figure 2.10, much the same as they would be to the post in the field. The mast arms were cut to an appropriate length and directly bolted to a 24 inch by 24 inch by 1 ¼ inch base plate that was itself attached to the backstop. This plate had various hole configurations to accommodate the varied bolt patterns of the different mast arms.

A hydraulic actuator was used to impart vertical loads in a cantilever action 80 inches from the weld on the mast arm as demonstrated in Figure 2.10. The actuator applied a dead load necessary to create a measured stress of 14 ksi at the top of the arm at the weld location. The 14 ksi dead load was determined to be representative of the dead load stress experienced by mast arms in service. This was calculated by using the dead loads on the two mast arms used during the field-testing, and determining the corresponding stress. Both arms had dead load stresses in the range of 14 ksi to 15 ksi.

The actuator applied a sinusoidal cyclic loading to create a measured stress range of 8 ksi to simulate constant fatigue loading cycles. Therefore, the maximum actuator load created a maximum stress of 18 ksi and the minimum load caused a minimum stress of 10 ksi. The 8 ksi stress range was chosen by using the design curve for a Category E' connection detail, shown in Figure 2.11. From the mean curve, it was determined that an 8 ksi stress range should cause a detectable crack at 1.6 million cycles. This number of cycles was a practical number to use at a significant stress range to examine the fatigue resistance and fatigue cracking. It would not

require the testing of a single specimen to last for months, yet it would not be of such short duration that comparisons could not be made.

The sinusoidal loading was applied at two cycles per second (Hz): below the natural frequencies of the test frame of approximately three hertz. At two hertz, a test usually required approximately ten days to reach 1.6 million cycles, including down time to check for cracks. Alderson (1999) presents the careful control for maintaining the dead load and cyclic stresses and for determining first cracking.

Strain gages were placed on the specimen four inches from the weld as they were on the mast arms in the field. The servo-controlled loads were set so that the top strain gage was measuring the desired stresses: 14 ksi average and 8 ksi range at the weld. Every four to six hours, data was collected to ensure stresses were within an acceptable range of the desired stresses. If the stresses were greater than one-tenth of a ksi from the desired stress, the loading was adjusted.

Magnetic Particle testing and visual inspection were used as a physical method to detect cracks. Mr. Vernon Hartman, an experienced inspector with the Missouri Department of Transportation, performed Magnetic Particle testing every 200,000 cycles or earlier if it was believed a crack had formed. Crack initiation could also be detected by examining the strains. As a crack formed, there was a local stiffness reduction. This reduction produced a change in stress at the gages. Although slight modifications of the loads were necessary during the testing period, an obvious trend of increased loading indicated the initialization of a crack. This was confirmed by, and it confirmed, the Magnetic Particle and visual inspections.

2.3.2 Laboratory Fatigue Test Results

Table 2.1 shows the results of the five mast arm fatigue tests. All of the mast arms were circular in section, except the JEM had an octagon section. One of the three Valmont mast arms failed well prior to the theoretical Category E' 1.6 million cycles. It also happened to be welded with the "fatigue-resistant" detail. Two of the Valmont arms, one with the new and one with the old weld detail, survived past the mean Category E' 1.6 million cycles. The Union Metals mast arm failed early as did the JEM arm. Both used the old weld detail. The JEM arm seemed to be cracked at the start of the test with no cycles prior to evidence of a crack. All fatigue failures propagated from the toe of the weld at the top of the mast arm at the maximum tensile stress locations for the circular sections and at the corners for the octagon section. Figure 2.12 shows the crack at the toe of the weld in Valmont mast arm 254682.

Table 2.1 Laboratory Mast Arm Test Results

Mast Arm	Manufacturer	Weld Type	Failure Cycles	Comments
254682	Valmont	Old	1.8 million	None
BB 34970	Valmont	New	2.1 million	None
CB 12917	Valmont	New	0.4 million	Possible lack of fusion of weld
88791	Union Metals	Old	0.5 million	Flaw detected by Mag Particle prior to loading
9539 CL54	JEM	Old	0.0 million	Flaw detected by inspection prior to loading

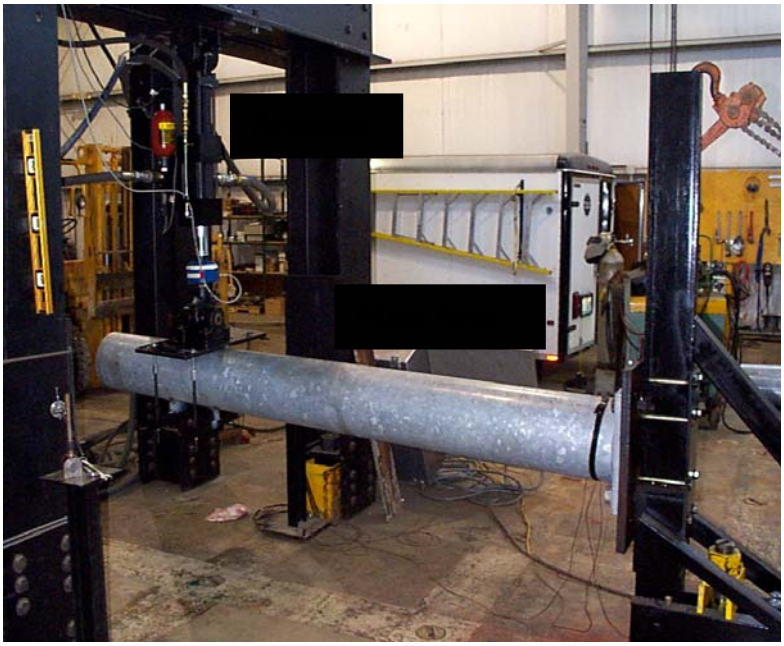

Figure 2.10 Test Set-Up for Fatigue Tests Valmont Mast Arm CB 12917

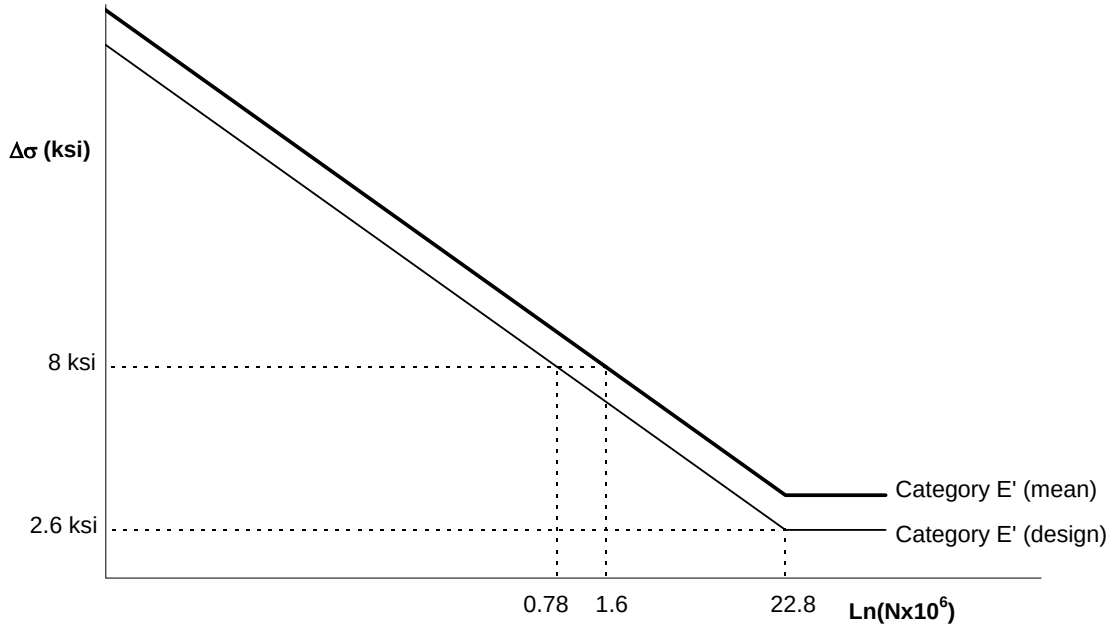

Figure 2.11 Fatigue Resistance of Category E' Detail

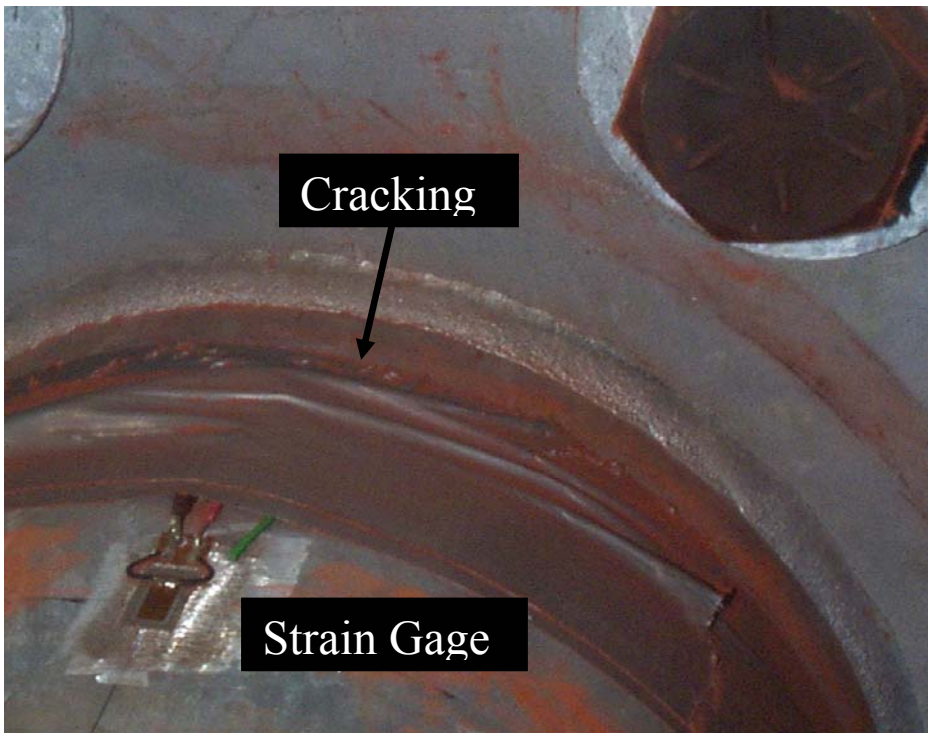

Figure 2.12 Valmont Mast Arm 254682 Cracking and Strain Gage

2.3.3 Metallurgical Failure Analysis

Two mast arms, CB 12917 and 254682, tested to failure in laboratory were analyzed for the cause of their failure. The first arm was designed with the new weld profile specified by the Missouri Department of Transportation while the second was designed with the old weld profile. However, the former failed at 0.4 million cycles and the latter failed at 1.8 million cycles. Both arms were metallographically examined to determine the morphological features associated with the weldments and the crack initiation site.

The same procedure as used to prepare for specimens of the in-service failed arm was followed to make two specimens from the cracked section. Both factographic and metallographic analysis were conducted on the specimens. The fracture surfaces indicate that the fatigue crack in both specimens initiated in an area at the weld toe of the mast arm. Classic features of fatigue fracture are present.

The most likely area for crack initiation was removed from the two specimens first by oxyacetylene cutting a relatively large piece from each of the mast arm assemblies. The "flame cut" pieces were then cut in an abrasive saw to remove specimens small enough to be used in a metallographic analysis. In addition, the metallographic specimens were sufficiently removed from the heat affected zone from the flame cutting operation in order to reveal the "as received" microstructure. Standard metallographic preparation procedures, as briefly described in Section 2.2.1.3, were employed in order to reveal the microstructure of the specimens.

The microstructures of both specimens are typical of low carbon steel. The base material is a low carbon ferrite – pearlite steel. The weld metal consists of large columnar grains containing acicular ferrite with bainite, consistent with the previous metallographic analysis of the in-service failed mast arms. The heat affected zone is also consistent with previously

reported data. The coarse grained region adjacent to the fusion line consists of blocky ferrite and bainite with some acicular ferrite. Further removed from the fusion line is the grain refined zone and finally the base metal.

The fatigue cracks in both specimens initiate at the toe of each weld in the mast arm. Specifically, the initiation site is at the toe of the weld at the junction of the weld metal and the coarse grained region.

The toe of the welds appears to have very sharp local toe angles. While it is not possible to directly measure the toe angle at the fracture initiation site, it is possible to examine the toe of the weld at the opposite side of the weld. The examination reveals that the sharp features found in the previous specimens cut from the in-service failed mast arms are nearly exactly reproduced in the two specimens. Both specimens are multi-pass weldments and appear to be "two pass" weldments. However, the advantages gained by the "fatigue-resistant" weld are negated due to the sharp features at the toe of the weld. Mast arms manufactured in this manner will continue to have less than expected fatigue life values as long as these sharp features at the toe of the welds are present. Even though the fatigue resistant welding procedure is utilized, the sharp features at the toe of the weldments will control the crack initiation or fatigue life.

In order to eliminate the sharp features of the weld, a thorough investigation of welding parameters must be accomplished. The optimum potential and current must be identified and combined with stringent quality control measures in order to eliminate these defective features in the weldments.

There is no information available for this study regarding to the specific welding process or welding procedures used in the manufacture of the mast arms under investigation. The welds appear to be produced using either the shielded metal arc process (SMAW) or the gas metal arc process (GMAW). The GMAW process is also known as the metal inert gas process (MIG) when an inert cover gas is used. In either case, oxide (rust) must be thoroughly removed from the components prior to the first weld pass, and any slag (SMAW) or thin oxide layer (GMAW) must be thoroughly removed between passes. In addition, it is very important that the proper welding potential be utilized (i.e., voltage). In particular, the effect of voltage on weld profile is dramatic and has been investigated by Frost and Olson at the Center for Welding Research at the Colorado School of Mines. The welding current essentially controls the heat input to the weld and thus the size of the weld. It does not have a significant effect on the weld profile.

In both specimens, the failure mechanism is identical to the specimens from the failed mast arms that were previously examined in this study. It results from the same type of sharp features at the toe of the weldments.

2.4 Summary

Based on the examination conducted, several observations are summarized below:

1. Failure of the signal mast arm initiated by fatigue cracking on the outside weld at the weld toe. Crack initiation was enhanced by the presence of weld undercutting, creating a sharp geometrical stress concentration. The location of the undercutting at the heat affected zone of the base material, where the base material is softest, further contributed to early fatigue failure.

2. The welds were of poor quality and exhibited lack of penetration and lack of fusion. However, this lack of penetration and lack of fusion did not contribute directly to the premature failure of the signal mast arm.
3. The weldments of the two mast arms tested to failure in the laboratory and analyzed have sharp features very similar to those examined for the in-service failed arms. Their failure mechanisms are thus the same even though one of the arms tested to failure in laboratory were designed with the new weld profile.
4. Laboratory tests indicated that two out of the three mast arms manufactured by Valmont company performed satisfactorily while both arms manufactured by JEM, Inc. and Union Metals, respectively, failed prematurely. Test results also verified that the new weld profile does not necessarily delay the initiation of cracking in mast arms.
5. The forensic investigation on the two arms tested to failure in the laboratory indicated that both have poor weld quality and fracture due to initiation of the crack at the weld toe though the laboratory tests resulted in quite different fatigue strength. The difference in fatigue strength (number of cycles) of the two arms is likely due to other factors that were not taken into account in the forensic investigation, such as residual stress on the base metals.

3. NEW AASHTO GUIDE SPECIFICATIONS

Signal and sign support structures are traditionally designed for material strength only (AASHTO, 1994). Recently, the support structures must also be in compliance with the fatigue criteria (AASHTO, 1999). The fatigue requirements were proposed based on a recent study by Kaczinski *et al* (1998). In this study, the potential impact of the new AASHTO Specifications on the fatigue analysis of existing mast arms and the design of new traffic sign supporting structures are evaluated. The Bridge Division at MoDOT is in the process of revising its standards to adhere to the new AASHTO Specifications.

3.1 Impact on Existing Mast Arms

The fatigue stress level of one of the failed signal support structures was checked against the proposed standard Specifications for Structural Supports for Highway Signs, Luminaires, and Traffic Signals (AASHTO, 1999). The post and the mast arm of the traffic signal support structure examined are tapering octagonal steel pipes. They have dimensions of 12"×11"×16.5'×7GA and 9.5"×3.5"×38'×7GA, respectively, and were manufactured by JEM Engineering & Manufacturing. The cantilevered structure was considered to support traffic signs on a major highway and classified as a Category I structure.

The signal mast arm is potentially subjected to four types of wind effects including galloping, vortex shedding, natural wind gust and truck-induced gust. The equivalent static wind loads and their corresponding stress levels at the arm-to-post connection are calculated. The maximum stress of 19 ksi was found as a result of the galloping effect (see the detailed calculations that follow). Since the welding detail at the connection belongs to Category E', the Constant-Amplitude Fatigue Threshold (CAFT) is only 2.6 ksi. This level of allowable fatigue stress is significantly below the calculated stress. Therefore, the arm-to-post connection is fatigue inadequate according to the Specifications.

Even if the support structure were installed at a local street and classified as Category III, the maximum equivalent stress at the connection could be as high as 6.6 ksi, resulting from the truck-induced wind gust. This stress level still exceeds the CAFT considerably and the connection is clearly insufficient according to the new Specifications.

The detailed calculation of the fatigue stress of the mast arm structure is described below. The cantilevered structure is schematically shown in Figure 3.1.

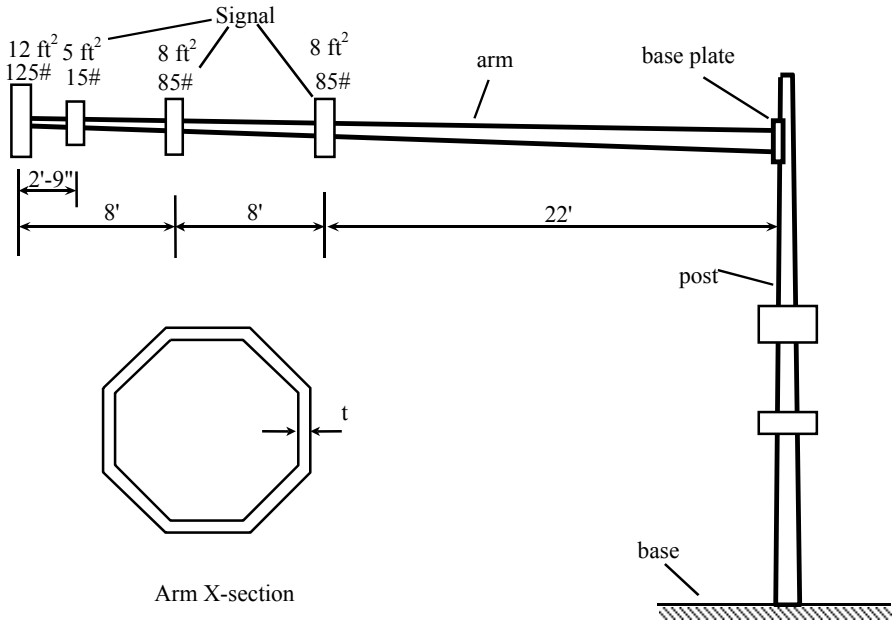

Figure 3.1 Sketch of the traffic signal support structure

(1) Dimensions

Pole -- 12"×11"×16.5'×7GA(0.1793")

Weight: 391lbs

C.G.: 8.13' from the base

Diameter of the post at the connection with the arm: 10.83"

Arm -- 9.5"×3.5"×38'×7GA(0.1793")

Weight: 510 lbs

C.G.: 16.1' from the base plate

R_c=(9.5"-0.1793")/2=4.66"

A_c=6.63Rt=6.63 ×4.66 ×0.1793= 5.54in^2

I_c=3.50R^3t=3.50 ×4.66^3×0.1793=63.50in^4

S_c=3.50R^2t=3.50 ×4.66^2×0.1793=13.63in^3

Signals and Signs

The vertical effective projected areas are respectively

A_1=A_2=8ft^2, A_3=5ft^2, A_4=12ft^2

(2) Loads

The structure is classified as Category I

a) Galloping

Importance factor: $I_F = 1.0$

Wind pressure: $P_G = 21\ I_F = 21$psf

For the corresponding signals/signs, the wind loads are

$F_{G1} = P_G A_1 = 21 \times 8 = 168$ lbs

$F_{G2} = P_G A_2 = 21 \times 8 = 168$ lbs

$F_{G3} = P_G A_3 = 21 \times 5 = 105$ lbs

$F_{G4} = P_G A_4 = 21 \times 12 = 252$ lbs

b) Vortex Shedding

According to Table 11.1 in the Specifications, the structure is not susceptible to this type of load.

c) Natural Wind Gusts

Importance factor: $I_F = 1.0$

Wind drag coefficient: $C_d = 1.2$ (for signal and octagonal cross-section arm)

Then the wind pressure is

$P_{NW} = 5.2 C_d I_F = (5.2)(1.2)(1.0) = 6.24$ psf

The horizontal wind forces on the structure are

$(F_{NW})_{arm} = P_{NW}(A_{arm})_V = P_{NW}(L_1+L_2+L_3)d_{average} = (6.24)(38)(9.5+3.5)/2/12 = 128.4$ lbs

$(F_{NW})_{signal1} = (F_{NW})_{signal2} = P_{NW} A_1 = (6.24)(8) = 49.9$ lbs

$(F_{NW})_{signal3} = P_{NW} A_3 = (6.24)(5) = 31.2$ lbs

$(F_{NW})_{signal4} = P_{NW} A_4 = (6.24)(12) = 74.9$ lbs

d) Truck Gust

Importance factor: $I_F = 1.0$

Wind drag coefficient: $C_d = 1.2$ for signal and octagonal arm

Wind pressure: $P_{TG} = 36.6\ C_d\ I_F = (36.6)\ (1.2)\ (1.0) = 43.9$ psf

Since the horizontal effective projected areas were not available, they are assumed as 1 ft^2, 1 ft^2, 0.5 ft^2 and 1 ft^2, respectively.

Then the wind forces on signals/signs are

$F_{TG1} = F_{TG2} = F_{TG4} = P_{TG} A_{h1} = 43.9$ lbs

$F_{TG3} = P_{TG} A_{h3} = (43.9)\ (0.5) = 22.0$ lbs

The truck-induced wind force is assumed acting on the outer 12 feet of the mast arm.

$d_{average} = (5.4+3.5)/2 = 4.5$"

$F_{TGarm} = P_{TG}\ (12)\ (4.5)/12 = 197.6$ lbs

(3) Moment at the arm-to-post connection

a) Due to Galloping

$(M_z)_G = \Sigma F_{Gi} \cdot x_i = (168)(22)+(168)(30)+(105)(38-2.75)+(252)(38)$

$= 2200$ lbs $\cdot$ ft $= 22$ kips $\cdot$ ft $= 264$ k $\cdot$ in

b) Due to natural wind gusts

The load on the arm acts at C.G.

$(M_y)_{NW} = \Sigma F_{NWi} \cdot x_i = (128.4)(16.1)+(49.9)(22+30)+(31.2)(35.25)+(74.9)(38)$

$= 8608$ lbs $\cdot$ ft $= 86.08$ kips $\cdot$ ft $= 103.3$ k $\cdot$ in

c) Due to truck gust

$(M_z)_{TG} = \Sigma F_{TGi} \cdot x_i = (197.6)(38-6)+(43.9)(30+22)+(22)(35.25)+(43.9)(38)$

$= 11050$ lbs $\cdot$ ft $= 133$ k $\cdot$ in

(4) Stress at the connection

From (3), it can be seen that the galloping load controls.

$\sigma_c = (M_z)_G / S_c = (264 \text{ k} \cdot \text{in}) / (13.62 \text{ in}^3) = 19.38$ ksi

Use the fatigue detail 16 with stress category E' (AASHTO, 1999)

CAFT $= 2.6$ ksi < 19.38 ksi

(5) Stress at the connection if the structure is considered as Category III

a) Galloping: $I_F = 0.3$

$M_z = (0.3)(264) = 79.2$ k $\cdot$ in

b) Natural wind gusts: $I_F = 0.59$

$M_y = (0.59)(103.3) = 61.0$ k $\cdot$ in

c) Truck Gust: $I_F = 0.68$

$M_z = (0.68)(133) = 90.4$ k $\cdot$ in Truck gust controls.

Max. Stress $\sigma_c = (90.4)/(13.62) = 6.6$ ksi $>$ CAFT $= 2.6$ ksi

(6) Conclusion

The connection is fatigue inadequate.

3.2 Impact of AASHTO Specs on New Design of Mast Arms

A proposed mast arm design method for fatigue was developed in NCHRP Report 412 (Kaczinski et al, 1998) and subsequently proposed in an AASHTO (1999) Guide Specification. Equivalent static loads were developed for the four types of dynamic loading: galloping, vortex shedding, natural wind gusts and truck induced gusts. These loads are applied to the areas of the mast arm and its attachments; and a bending stress is determined, which is compared to the constant amplitude fatigue limit (CAFL) for the appropriate connection detail. Importance categories and factors were developed for the different safety and performance criteria.

Importance factors are introduced to adjust the level of reliability of cantilevered mast arms. Based on the satisfactory performance of most arms throughout the past, it was concluded

that not all cantilever support structures need to be redesigned. However, due to the recent failures, a more rigorous design for fatigue is necessary for more critical structures (Kaczinski et al, 1998). The different load types are also given different levels of importance within each importance category. Galloping has greater importance than wind gusts or truck-induced gusts because it could quickly lead to failure. Natural wind gusts and truck-induced gusts are expected to produce significant responses randomly. Therefore, damaging cycles are less likely to occur than those experienced by a mast arm susceptible to galloping.

Category I is for critical cantilevered support structures on major highways. The full magnitudes of the equivalent static loads are applied to the structure. The member size is determined to insure these loads do not exceed the CAFL. Members designed for Category I will need to be substantially increased in size. This is evident from the design check in Section 3.1. Structures designed for Category I should not exhibit fatigue problems during their service life.

Because most arms perform satisfactorily, lesser importance categories were established. Category III, which is for the least critical structures, is intended to produce no significant increase in member size (Kaczinski et al, 1998). Category III was developed by examining the performance of existing structures compared to the proposed specification. The performance ratios, the ratios of the CAFL to the stresses obtained using the proposed specification, were used to establish reduction factors. These factors are applied to reduce the equivalent static loads such that the current design would be satisfactory. Thus, members designed for Category III should not need to be increased in size. However, the structure would have the same reliability as current structures; and premature failures may be expected.

Category II was established to provide a middle level of importance between the extremes of Categories I and III. Category II is for structures on major highways that are not classified as Category I and for structures on secondary highways. The importance factors were determined by averaging the importance factors of Categories I and III. This results in increases in member sizes, but not to the degree of Category I. However, structures designed for Category II may be subject to cracking. Therefore, a designer or department needs to determine how critical a structure is, and whether premature failures are acceptable. The increase in cost would also need to be evaluated against the increase in reliability of the structure.

According to the sample design in Section 3.1 and from studies by Alderson (1999), the proposed specifications would significantly increase the sizes of new mast arms. Alderson evaluated the field tested mast arms at Stadium and Forum and at Providence and Green Meadows. For all categories (I, II & III), the stresses were significantly larger than the CAFL. In redesigning the mast arms to the proposed specification, the sizes of the arms significantly increased for all three categories. Table 3.1 shows the mast arm diameter required for the two field test mast arms for the various categories in the proposed AASHTO design specification.

From Alderson's work with the analysis and redesign, it is apparent the current designs are insufficient for the proposed specification regarding fatigue. The proposed specification intends to make galloping the controlling load situation in Category I and II, but less important in Category III, which is the justification for the varying importance factors. This is demonstrated in the analyses when the highest stresses are for galloping in Category I and Category II. In Category III galloping may still control depending on the geometry of the arm and its attachments, but it will not exceed the stresses from the other types of loads greatly.

Another intention of the proposed specifications is that arms designed for Category III would not need to be much larger than current designs. However as the arm's size is increased,

the large area of the arm causes the moments due to natural wind and truck-induced gusts to increase while galloping moment remains unchanged. Thus, these forces begin to control instead of galloping. This seems contrary to the intention of the proposed specifications. Truck-induced moments increase the most because a larger equivalent static pressure is used for truck gusts than natural wind. In addition, a long mast arm would experience large moments due to the distance between the connection and the application of the forces. However, this would be less significant if the rate of taper was changed such that the member is larger in diameter at the connection, but relatively unchanged at the tip with respect to the current design.

3.3 Summary

The proposed specification provides a systematic method to design mast arms for fatigue. It also provides different importance categories for the reliability levels most appropriate to a particular structure. The current mast arm designs that were analyzed are not satisfactory for any of the load conditions in any of the importance categories. The designs presented using the proposed specification provide examples of how member sizes may be impacted by the proposed specification. Members would likely need to be increased two to three times to meet the necessary requirements. Contrary to the intention of the specification, truck-induced gusts control the design. Member sizes would need to be increased significantly even for Category III.

Table 3.1 Required Mast Arm Sizes with Draft AASHTO Specification

Mast Arm	Actual Size	Required Category I Size	Required Category II Size	Required Category III Size
Stadium & Forum	12.5 in	42.5 in	35.0 in	27.5 in
Providence & Green Meadows	9.5 in	27.5 in	22.5 in	17.5 in

4. IN-SERVICE LOADING

This section is focused on developing two models for truck and natural wind-induced loading according to the field test data. Toward the end of this section, the vulnerability of two in-service signal support structures to galloping is also assessed.

4.1 Truck-Induced Loading

4.1.1 Truck/large-vehicle field tests

The aim of this task is to set up an appropriate truck-induced gust model and calibrate it with the field test records (Alderson, 1999). A series of field tests have been conducted on two traffic signal support structures in Columbia, MO. One structure is located at Stadium (Rt. 740) & Forum Blvd, manufactured by Valmont Industries. Its elevation is schematically shown in Figure 5.1. Both the mast arm and post have circular cross sections of size 12.5"×4.65"×54'×7GA(0.1793") and 14.5"×11.4"×27'×0.2188", respectively. The luminaire arm is 4.17"×2.38"×11GA. The specific geometry and weight of various components of the signal and sign supporting structure are summarized in Table 4.1.

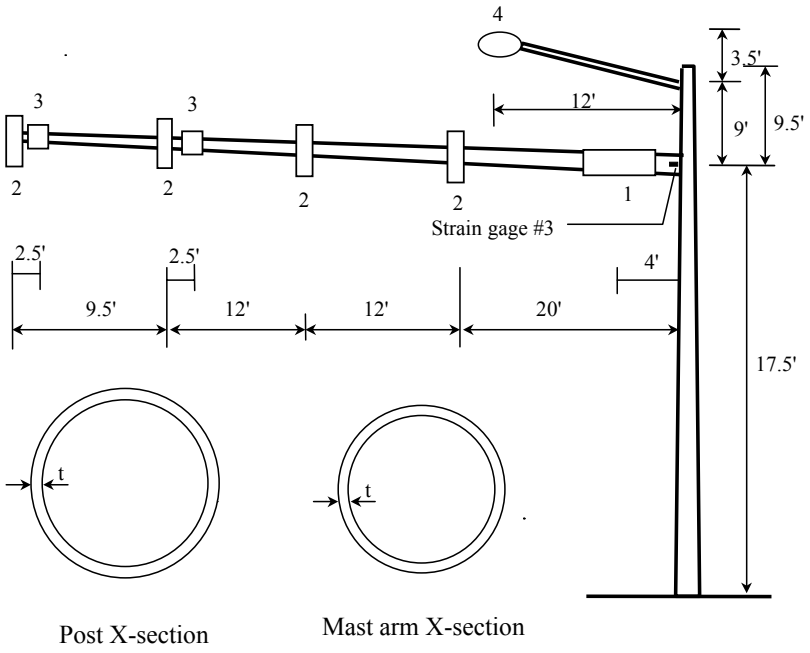

Figure 4.1 Traffic signal support structure at Stadium & Forum

Table 4.1 Geometry and weight of the signal mast arm at Stadium & Forum Blvd.

No.	Description	Weight(lbs)	Vertical Projected Area (ft^2)	Surface Area (ft^2)
1	72"×18" sign	20	9	----
2	3-section O.L. head	40	8.67	32.5
3	24"×30" sign	27	5.0	----
4	Luminaire	60	3.3	----

The other structure is located at Providence (Rt. 163) & Green Meadows Rd, which was manufactured by JEM Engineering. Its elevation is shown in Figure 5.2. The mast arm is octagonal and the post is circular. They are respectively 10.5"×3.5"×42'×7GA(0.1793") and 14.25"×11.5"×27.5'×0.2188". The luminaire arm was built with a 2" schedule 40 pipe. The geometry and weight of the supporting structure is given in Table 4.2.

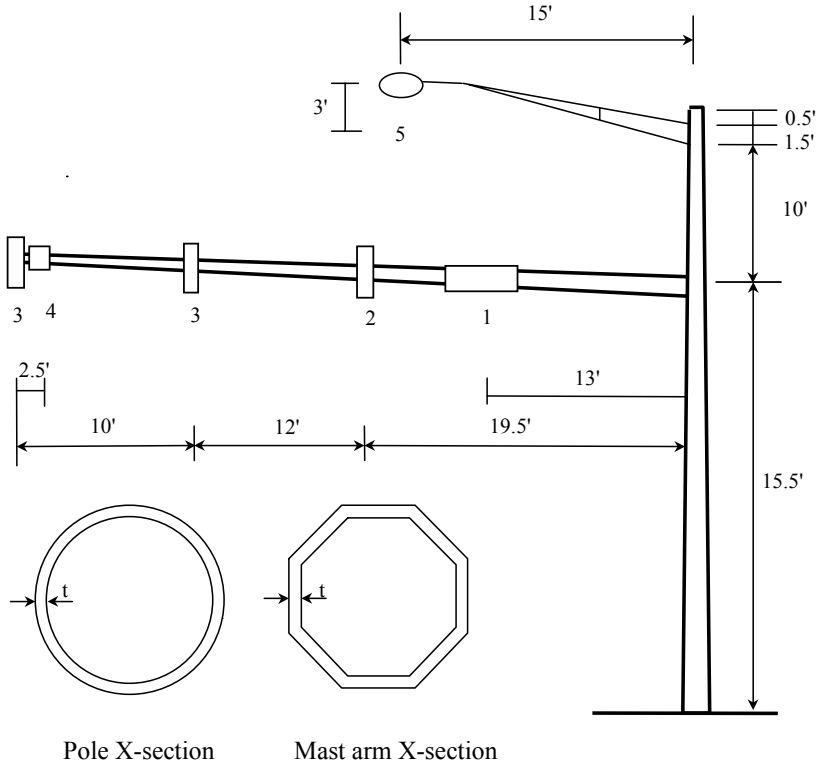

Figure 4.2 Traffic signal support structure at Providence & Green Meadows

Table 4.2 Geometry and weight of the signal mast arm at Providence & Green Meadows Rd.

No.	Description	Weight(lbs)	Vertical Projected Area (ft^2)	Surface Area (ft^2)
1	120"×18" sign	25	15	----
2	5-section O.L. head	100	12	47.5
3	3-section O.L. head	50	8	32.5
4	24"×30" sign	27	5	----
5	Luminaire	60	3.3	----

The acceleration at the end of the cantilevered arm and the strains at the mid-span of the arm and the arm-to-post connection were measured in field conditions. Among them, only the strain data provide useful information for further investigation due to malfunction of the accelerometers. There are 12 strain gages on each mast arm. They are deployed as indicated in Figure 4.3.

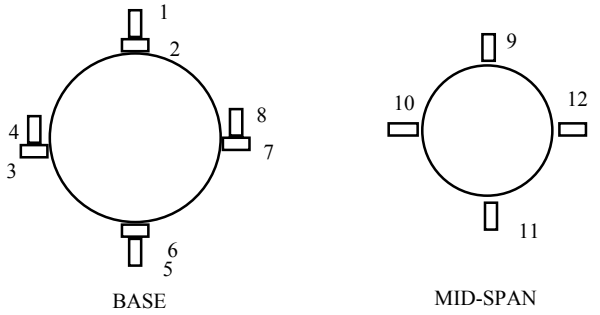

(a) Stadium & Forum St.

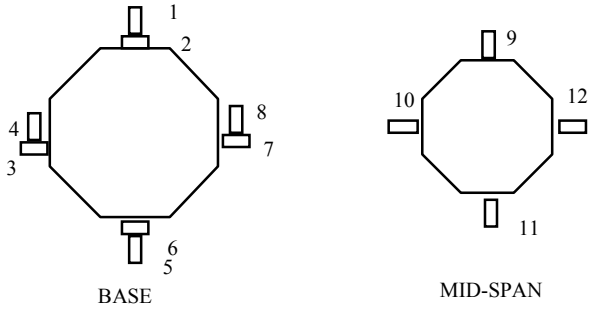

(b) Providence & Green Meadows Blvd.

Figure 4.3 Location of strain gages

The field tests were conducted on the two structures three times in 1999: May 15, July 1 and December 7. A total of 26 events (data files) were recorded. The July 1 and December 7 tests were done using a test truck of known dimension and weight while the May 15 tests depended on passing vehicles. Most of the records due to the test-truck-induced vibration indicated insignificant truck loading effects. The reasons may lie in several aspects. The test truck used during the tests does not have the box-like trailers in the back. Its windward surface is thus significantly smaller in size than a commercial truck with a long box-like trailer. The speed limit of the street/highway is only 45 mph at the test site. Therefore, it is difficult to have the test truck generate the wind gust of expected intensity. For example, the maximum strain magnitude is only several micro-strains on the mast arm at Providence & Green Meadows Rd., which corresponds to a stress of less than 1/3 ksi. For these reasons, the field test results corresponding to the test truck-induced wind gust were not used in the analysis.

The May 15 tests (7 events) were conducted on the mast arm at Stadium & Forum. The vibration of the arm is induced by several passing vehicles. The strain magnitude in these records is relatively large. However, when compared with the video footage recorded during the tests, no significant vibration was observed corresponding to most of the time history records. One record indicates the appreciable gust effect of passing vehicles. Unfortunately, the corresponding video footage was accidentally overwritten on the tape so that no information on traffic condition was actually obtained. According to the field notes, the severe vibration of the arm is most likely due to the passage of a long bus. The following analysis on the truck-induced gust is mainly based on this record.

4.1.2 Modeling of truck-induced loading

As mentioned in the preceding section, only one record shows a significant gust effect. It represents the longitudinal strain on the front face of the arm-to-post connection at gage #3 as indicated in Figures 4.1 and 4.3(a). The strain response was converted to stress, which is plotted in Figure 4.4. Since the peak response occurs at approximately 80 s, the wind load from 60 s to 100 s is focused on below.

The signal support structure at Stadium & Forum Blvd. was modeled and analyzed using the SAP2000 Nonlinear software. Figure 4.5 presents the finite element model of the structure. Under normal operational conditions, the support structure is subjected to both truck and natural wind-induced loading. The natural wind gust is assumed to distribute uniformly along the entire length of the arm. The truck-induced gust, however, depends on the traffic lane arrangement of the highway. For simplicity, the truck gust pressure is assumed to act uniformly on the middle portion of the arm, 12' to 44' away from the base, both in horizontal and vertical directions. The gust pressure distribution is shown in Figure 4.5. The horizontal effective projected area is assumed to be 2 ft^2 for each signal.

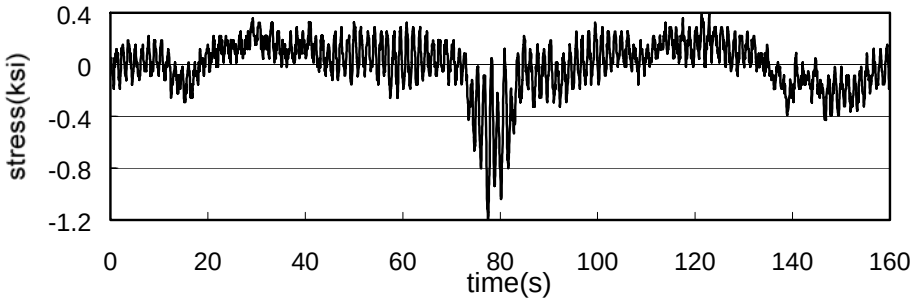

Figure 4.4 Stress time history at strain gage #3

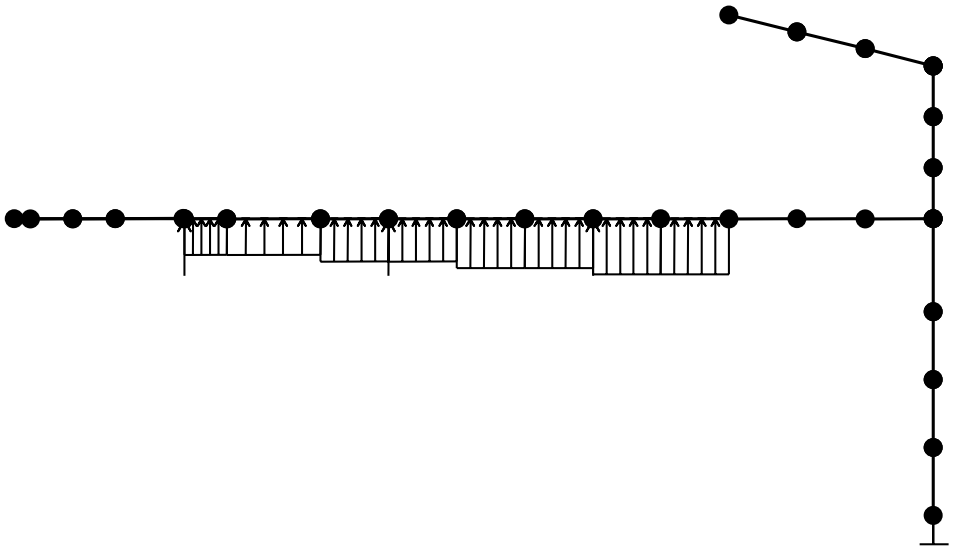

Figure 4.5 Structural model for SAP 2000 Nonlinear Analysis

The natural frequencies and vibration modes of the structural model were calculated. The fundamental period of 1.34 sec corresponds to the out-of-plane motion associated with the torsional effect of the post while the 2nd mode of period 1.28 sec represents the in-plane motion due to bending in the arm and post of the signal support structure. The fundamental period agrees well with the time elapsed in each cycle of the measured response as indicated in Figure 4.4.

Time-history analysis was conducted to simulate the truck-induced gust loading. Due to the missing information on the passing vehicle, it is difficult to calibrate any gust load model with test data. In what follows, a trial-and-error method is used to determine the gust pressure on the signal and sign support structure.

The truck-induced wind gust can be regarded as a triangular impulse with a total duration of 0.375 sec (0.125sec+0.25sec) as illustrated in Figure 4.6 (Creamer *et al*, 1979). The peak value of the gust pressure is 1.23psf. The longitudinal stress response at gage #3 due to this impulse load is presented in Figure 4.7. The impulse was considered to arrive at the 10th second. However, by comparing Figure 4.7 with Figure 4.4, it can be clearly seen that the peak response from 70s to 90s in Figure 4.4 was not induced by the gust of one truck only. The response recorded from the field test is most likely due to several truck gusts along with the natural wind effect.

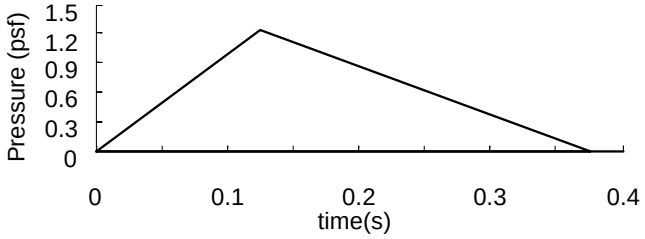

Figure 4.6 Truck-induced gust model

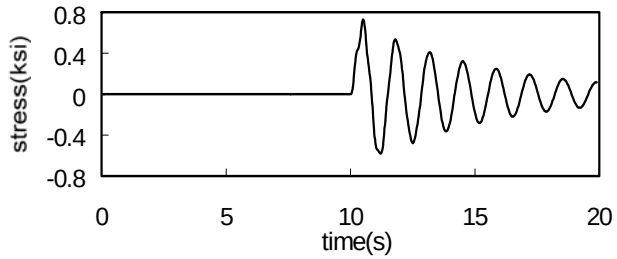

Figure 4.7 Stress at gage #3 due to the gust impulse in Figure 4.6

The wind load can be regarded as the superposition of average wind and wind fluctuation. In this study, the average wind load was first extracted from the strain record measured at gage #3. Then, various pulse trains were used to simulate the wind fluctuation and truck-induced gust effect. The particular pulse train that leads to the structural responses in good agreement with the test data is referred to as the synthesized wind pressure and is shown in Figure 4.8. The stress history due to the synthesized wind load is compared in Figure 4.9 with the test results measured at gage #3. It can be observed from Figures 4.8 and 4.9 that the peak response from 70 to 90 sec was mainly caused by four wind gusts at approximately 74, 77, 80

and 82 sec due to natural wind or truck passage. Considering a speed limit of 45 mph on the highway/street, the distance between two trucks was roughly estimated as 150~200 ft, which is reasonable for the four-lane highway.

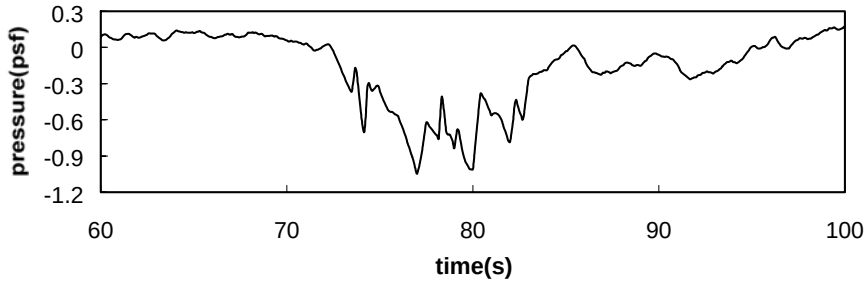

Figure 4.8 Synthesized truck-induced gust

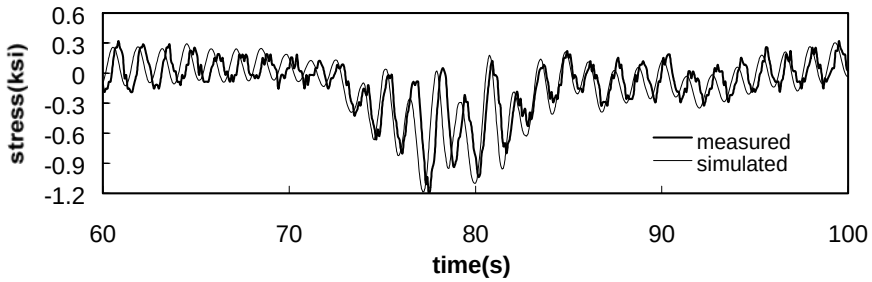

Figure 4.9 Measured and the simulated stress response at gage #3

The damping ratio of the signal support structure was identified as 4% from the truck-induced motion. This value seems too high for a steel cantilever structure. It may be because several trucks can counteract their effect on the response of a signal and sign support structure when they drive through the structure on multiple lanes in a stagger pattern. The reduced gust effect is interpolated in numerical analysis as the increase in damping. To fully calibrate the truck-induced gust model, more complete field test data are required. The test truck must carry a full-size trailer to generate substantial wind effects on signal mast arm structures.

4.1.3 Discussions on new AASHTO Specifications

According to the recently approved Specifications (AASHTO, 1999), truck-induced gusts mainly cause the vertical vibration of signal and sign support structures. This conclusion and its associated design requirements do not agree with some of the recent research results.

Gray *et al* (1999) stated "that the vertical movement is caused primarily by galloping and that the horizontal movement is caused by natural and truck induced gusts." Creamer *et al* (1979) also stated that " Because the area of the sign face is much larger than that of the lighting case area, horizontal motion dominates, as observed in the field tests." Similarly, this study has shown that the stress at gages #3 and #7 are the largest among the 12 locations indicated in Figure 4.3. These results suggested that the horizontal vibration induced either by truck passing

or natural wind is more significant than the vertical vibration. Galloping was not observed during the monitoring period of two mast arm structures.

In the report by Creamer *et al* (1979), the maximum gust pressure induced by a truck moving at 50mph is only 1.23 psf. However, the recently approved Specifications required that traffic sign structures be designed for a truck-induced pressure of 29.8 psf even when the structures are classified as Category III. Although these two stresses have different meanings, the substantial discrepancy suggests that the truck-induced wind load required by the Specifications be subject to further verification.

4.2 Natural Wind-Induced Loading

4.2.1 Methodology

The objective of this task is to estimate the natural wind-induced stress on signal mast arms for fatigue analysis. A statistical procedure is developed based on the field test data. Fatigue failure of a properly designed and carefully constructed structure usually takes place after a long period of service. It results from the accumulated effect of a significant number of minor damages. Therefore it is prudent to assume that, for the purpose of predicting the fatigue stress, natural wind gust are repeatable every ten years in a statistical sense.

As determined in the preceding section with a computer model, the fundamental period of mast arm structures is around one second. It is significantly less than the dominating period of natural wind fluctuation (Simiu and Scanlan, 1996). Therefore, except for the galloping or vortex shedding effect, wind fluctuation will not induce the resonant vibration of the mast arm structures. Such a structure mainly oscillates at its own fundamental period. Although depending upon the direction and angle of wind gusts, the dynamic responses of the mast arms are most likely proportional to the wind pressure or the square of the average wind speed. If the ratio between the wind-induced stress and the square of wind speed is of the similar statistical distribution for a range of the measured wind speeds, the same distribution can be reasonably extended to higher wind speed ranges that are rarely recorded in field tests.

The average wind speed distribution can be determined from the wind data collected at local stations near mast arm structures. Therefore, the distribution of structural responses such as stress range can be determined provided that the distribution is known under a given wind speed range. The latter information is obtained through field tests on the same two support structures as described in Section 4.1.1. The following procedure is recommended to estimate the number of stress cycles at various levels on a signal and sign support structure:

1. Analyze the historical wind gust records (10 years) in the vicinity of the structure to determine the statistical distribution of the wind speed.
2. Monitor the stress change of the structure in field conditions due to wind gusts of various speeds.
3. Determine the number of cycles at various stress levels (normalized by the square of wind speeds) from the field test data on the instrumented mast arm.
4. Extrapolate the stress distribution in Step 3 into that corresponding to the rare wind events of higher speed.
5. Compute the number of cycles corresponding to different stress ranges by multiplying the wind speed distribution by the load spectrum from Steps 3 & 4.

4.2.2 Wind speed distribution at Columbia, MO

The wind speed information at Columbia, MO, is provided by the National Climatic Data Center (NCDC, http://www.ncdc.noaa.gov). The data were collected during the period 1969 through 1978. They include the monthly and annual statistics on the occurrence of wind events at various hourly mean wind speeds in 16 horizontal directions. Appendix A lists the annual wind speed information collected from NCDC. Since there is no information on the wind direction in the field test on the mast arms, the wind gusts with the same speed were grouped into one category regardless of their direction. Figure 4.10 shows the annual statistics of wind speed, which mainly follows a logarithmic normal distribution.

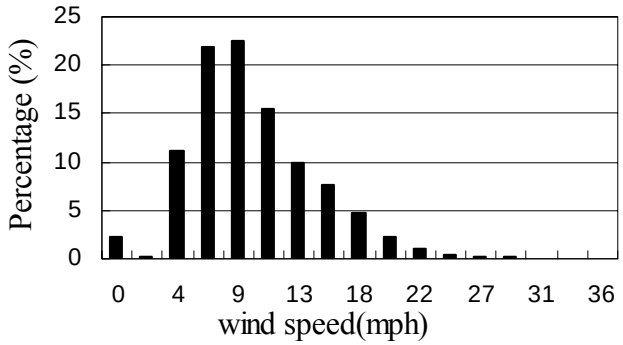

Figure 4.10 Annual wind speed statistics for Columbia, MO

4.2.3 Natural wind-induced field tests

Both mast arms at Stadium & Forum Blvd. and Providence & Green Meadows Rd. were instrumented as shown in Figure 4.3. A total of 31 events (518 seconds of accumulated time) were recorded for the signal support structure located at Providence & Green Meadows Rd. and 26 events (451 seconds of accumulated time) were recorded at Stadium & Forum. The wind speed, ν, measured during the tests ranges from 6 to 30 mph. Each structure was instrumented with twelve strain gages. Among the twelve strain records, the emphasis is placed on analyzing the responses at gages #1, 3, 5 and 7. They measured the longitudinal strains located at 4 in. away from the arm-to-post connection. Presented in Figure 4.11 is a typical stress time history at strain gage #3, which is converted directly from the measured strain at a wind gust of 16.4 mph.

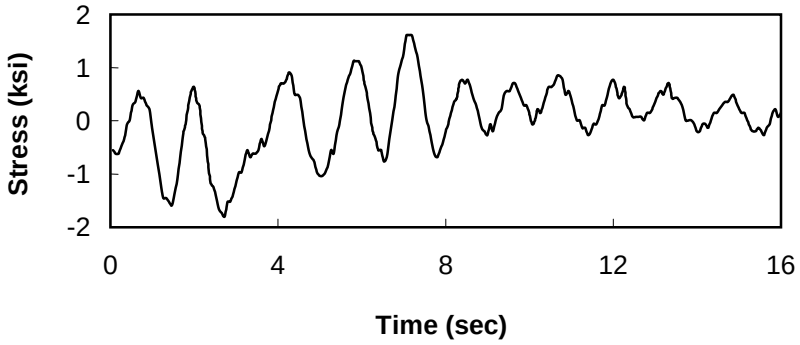

Figure 4.11 Stress time history at gage #3 due to natural wind gust

4.2.4 Horizontal vibration of mast arm

Strain gages #3 and #7 were used to measure the longitudinal strains at two sides of the mast arm near the base plate. The strains are associated with the out-of-plane (horizontal) vibration of the signal support structure. Since their responses are of the same magnitude, only the records at gage #3 are used for the following analyses.

4.2.4.1 Load spectrum due to natural wind gusts

To determine the fatigue load on the mast arm, the stress range from peak to valley of each cycle of vibration, as shown in Figure 4.11, is computed for every event. The minimum stress range considered in calculation is 0.5 ksi for the Stadium & Forum mast arm and 0.2 ksi for the Providence & Green Meadows mast arm. The total number of cycles can then be counted for each stress level and divided by the total test time to compute the occurrence per second. Figures 4.12 and 4.13, respectively, present the stress occurrence of the two structures as a function of stress level. They are referred to as load spectra.

To see whether the load spectrum shown in Figures 4.12 and 4.13 is representative for all wind gusts regardless of wind speed, the test data were grouped into three subsets according to their wind speeds. For the structure at Stadium & Forum Blvd., the wind speed of each subset ranges up to 13 mph, 13 to 16 mph, and greater than 16 mph. For the structure at Providence & Green Meadows Rd., it ranges up to 16 mph, 16 to 20 mph, and greater than 20 mph, respectively. The load spectrum for each subset can be determined in the same fashion. All three spectra, together with the overall spectrum, are compared in Figure 4.14 for the Stadium & Forum structure and Figure 4.15 for the Providence & Green Meadows structure. As one can see, they are very similar in terms of stress distribution, though small difference in detail exists at several points. Therefore, the response distribution in Figures 4.12 and 4.13 can be used for other wind speed ranges.

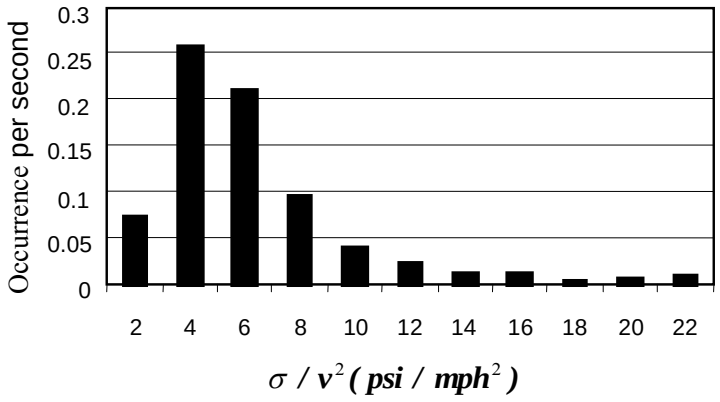

Figure 4.12 Longitudinal stress level distribution due to natural wind gust (Stadium Blvd & Forum)

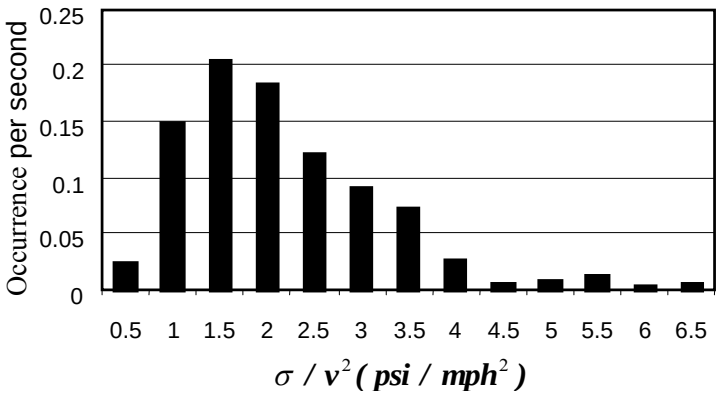

Figure 4.13 Longitudinal stress level distribution due to natural wind gust (Providence & Green Meadows)

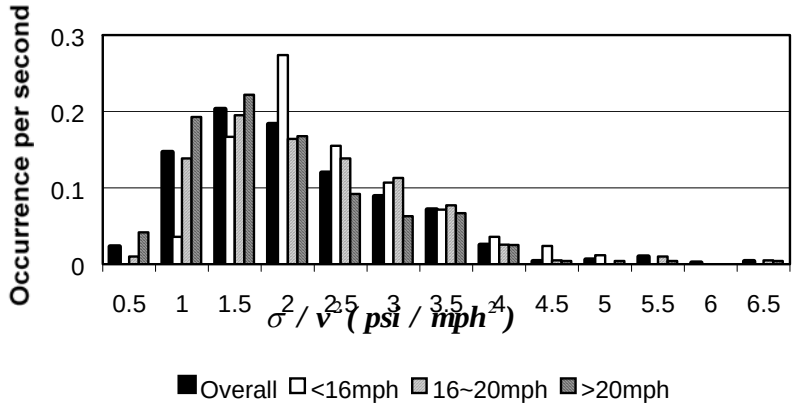

Figure 4.14 Response statistics based on different data sets (Stadium & Forum)

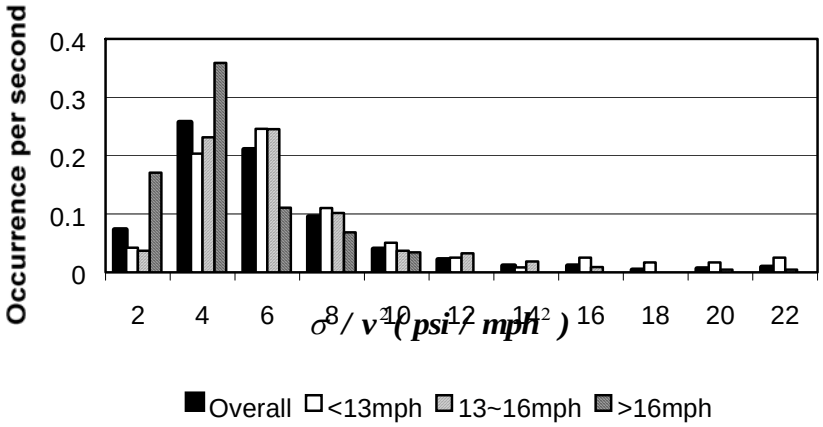

Figure 4.15 Response statistics based on different data sets (Providence & Green Meadows)

4.2.4.2 Annual number of cycles at various stress levels

The wind speed distribution presented in Figure 4.10 and the load spectra in Figures 4.12 and 4.13 are used to predict the number of cycles of vibration that a mast arm may be subjected to at different stress levels. For each wind speed from Figure 4.10, one can compute the occurrence frequency at various stress levels by multiplying the square of the wind speed by the ratio of stress over the square of wind speed in Figures 4.12 and 4.13. After every wind speed in Figure 4.10 is taken once, the occurrence frequencies corresponding to the same stress level are added into the total number of cycles per second. The annual number of cycles of vibration at various stress levels is then obtained. Table 4.3 gives the predicted annual occurrence of different levels of stress at the Stadium & Forum and the Providence & Green Meadows mast arms.

Table 4.3 Predicted number of cycles at various level of stress ranges per year

Providence & Green Meadows Blvd.		Stadium & Forum St.			
Stress level (ksi)	No. of cycles	Stress level (ksi)	No. of cycles	Stress level (ksi)	No. of cycles
<0.2	1.742×10^{7}	<0.5	1.404×10^{7}	14~16	7.807×10^{2}
0.2~0.4	5.515×10^{6}	0.5~1.0	5.412×10^{6}	16~18	6.934×10^{2}
0.4~0.7	3.401×10^{6}	1.0~2.0	2.559×10^{6}	18~20	5.825
0.7~1.0	9.522×10^{5}	2.0~3.0	8.401×10^{5}	20~22	8.159
1.0~1.5	4.648×10^{5}	3.0~4.0	2.445×10^{5}	22~24	4.663
1.5~2.0	1.269×10^{5}	4.0~5.0	1.086×10^{5}		
2.0~2.5	2.814×10^{4}	5.0~6.0	5.767×10^{4}		
2.5~3.0	1.289×10^{4}	6.0~7.0	4.335×10^{4}		
3.0~4.0	6.387×10^{3}	7.0~8.0	1.295×10^{4}		
4.0~5.0	1.207×10^{3}	8.0~9.0	8.216×10^{3}		
5.0~6.0	2.943×10^{2}	9.0~10	4.773×10^{3}		
6.0~7.0	3.044	10~12	5.378×10^{3}		
7.0~8.0	2.029	12~14	2.133×10^{3}		

4.2.5 Vertical vibration of the mast arm

The bending stresses at the top and bottom of mast arms are associated with the vertical vibration of the signal support structures. Such structures are atypically more flexible out of plane than in plane. It is likely that the horizontal vibration is stronger than the vertical vibration since its natural frequency is relatively closer to the predominant frequency in wind fluctuation. The field test data at gages #1 and #5 confirm that the stress associated with the vertical vibration is less than 1/3 of that with the horizontal vibration. Therefore, only the bending stress at the side of the arm-to-post connection needs to be considered for the assessment of fatigue life.

4.3 Potential for Galloping

Many investigations concluded that it is difficult to reproduce the galloping phenomena in lab and field conditions (Creamer *et al*., 1979; Gray *et al*., 1999). This study reinforces that statement since galloping was not observed throughout the field tests. Nevertheless, galloping

occasionally occurs in signal and sign support structures (Edmund, 1996). In what follows, the potential for galloping of the two mast arms instrumented in this study is evaluated theoretically.

Galloping is an instability phenomena associated with the decreasing of damping in structural systems due to aerodynamic effect. Across-wind galloping only happens to slender structures having special cross-sectional shapes. Structures with circular cross section are exempt from galloping (Simiu and Scanlan, 1996). Therefore, among the two structures instrumented in field tests, only the Providence and Green Meadows mast arm needs to be evaluated for potential galloping.

Based on Equation 6.2.12 in Simiu and Scanlan (1996), the equation of motion for the first mode of the mast arm with aerodynamic effect can be written as

$$m_1^*(\ddot{Y}_1 + 2\xi\omega_1\dot{Y}_1 + \omega_1^2 Y_1) = -\frac{1}{2}\rho U(\frac{dC_L}{d\alpha} + C_D)B_1^*\dot{Y}_1 \tag{4.1}$$

in which

$B_1^* = \int \phi_1^2(x)B(x)dx$

$m_1^* = \int \phi_1^2(x)m(x)dx$

$B(x)$: Diameter of the mast arm,

$m(x)$: Mass per unit length of the mast arm = $\pi\rho_s t\, B(x)$,

$\phi_1(x)$: Shape of the 1st mode,

ω_1: Circular frequency of the 1st mode (in-plane bending) = 5.7 rad/sec for the structure at Providence & Green Meadows Rd.,

Y_1: Generalized coordinate of the 1st mode,

ρ : Mass density of air = 0.0765lb/ft^3,

ρ_s : Mass density of steel = 486.7lb/ft^3,

U: Wind speed,

α : Attack angle of the wind,

C_L, C_D: Lift and drag coefficients.

The right-hand side of Eq. (4.1) represents the aerodynamic effect. By combining the aerodynamic effect into the mechanical damping effect, the total damping of the structural system is equal to

$$d = 2m_1^*\xi\omega_1 + \frac{1}{2}\rho U(\frac{dC_L}{d\alpha} + C_D)B_1^* \tag{4.2}$$

Galloping occurs when the total damping $d<0$. To approximately evaluate the possibility of galloping, the lift and drag coefficients for an octagonal section from Simiu and Scanlan (1996) were used. They are reproduced in Figure 4.16. According to this figure, a slender octagonal mast arm could be susceptible to galloping in certain attack angle ranges $(-5^\circ < \alpha < 5^\circ)$ because

$$\left(\frac{dC_L}{d\alpha}+C_D\right)_{\alpha=0} \approx -5.0+1.1=-3.9<0 \tag{4.3}$$

For the structure under consideration, the lower threshold wind speed for galloping can be estimated by letting Eq. (4.2) equal to zero. That is,

$$U_g = -4\pi\rho_s t\omega_1\xi/\rho\left(\frac{dC_L}{d\alpha}+C_D\right)\Big|_{\alpha=0} \approx 4\pi\times 486.7\times(0.1793/12)\times 5.7\xi\ /\ (0.0765\times 3.9)$$

$$=1746\xi \text{ ft/sec} = 1190\xi \text{ (mph)} \tag{4.4}$$

When ξ=4% as used in Section 4.1.2, U_g=48 mph. This result indicates that the signal support structure could be vulnerable to galloping under wind gusts of 48 mph or higher.

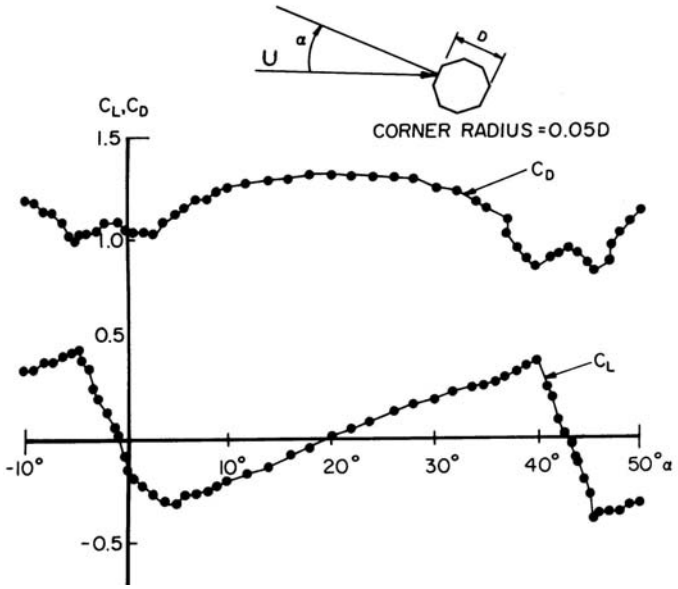

Figure 4.16 Force coefficients on an octagonal cylinder (Re=1.2×10^6)

4.4 Summary

The analysis conducted in this section lead to the following results:

1. Both the wind speed and the ratio between stress and the square of wind speed follow the logarithmic normal distribution. Since the ratio is insensitive to the wind speed, its distribution can be used for weak and strong wind gusts.
2. The average stress in the signal arm structure at Forum & Stadium Blvd. is significantly larger than that at Providence & Green Meadows Rd. due to its longer span length.
3. The intensity of vertical vibration caused by natural wind gusts is less than 1/3 of that of horizontal vibration.
4. The octagonal mast arm at Providence & Green Meadows Rd. is likely vulnerable to potential galloping induced by natural wind gusts.

5. FATIGUE AND REMAINING LIFE MODELS

5.1 Stress Analysis

According to the 1994 Standard Specifications for Structural Supports for Highway Signs, Luminaries, and Traffic Signals by NCHRP17-10, the following three types of loads are related to the fatigue design of the tapered structure of the Providence & Green Meadows Rd. The loads acting on the signs and the signals are considered as concentrated loads applied at the center of the mast arm where the signs and the signals are fixed, and the loads acting on the mast arm are considered as distributed loads. They are listed below:

Galloping: P_G=0.1458 psi
Natural Wind Gust: P_{NW}=0.0433 psi
Truck-Induced Gust: P_{TG}=0.305psi
Dead Loads: Sign 1: 16 lbs
Sign 2: 16 lbs
Sign 3: 10 lbs
Signals: 52 lbs.

5.1.1 Finite Element Model

A computer model (global model) of the entire mast arm structures was used to determine the global distribution of internal forces and moments under the above loads. Another computer model (local model) was set up to investigate the local distribution of stress around the arm-post weld connection. A 45-inch segment of the mast arm was cut and refined finite element meshes were generated for the segment with a detailed modeling of the weld profile. The cross sections of the arms investigated with ABAQUS are shown in Figure 5.1. It is noted that for the octagonal arm, a 0.625-inch radius was used to simulate the transition of the mast arm wall around the corner of the octagonal section for a realistic modeling. This treatment also eliminates the singularity of the stress amplitude in numerical computation. It was observed from field inspections that the weld leg of the instrumented structures is typically 1/4 inch long on the base plate and 7/16 inch long on the mast arm wall. There are over 36,000 three-dimensional solid elements with minimum element size of $0.04'' \times 0.04'' \times 0.4''$. The external loads on the refined model are the forces and moments at the cut section of the entire signal structure from the global model.

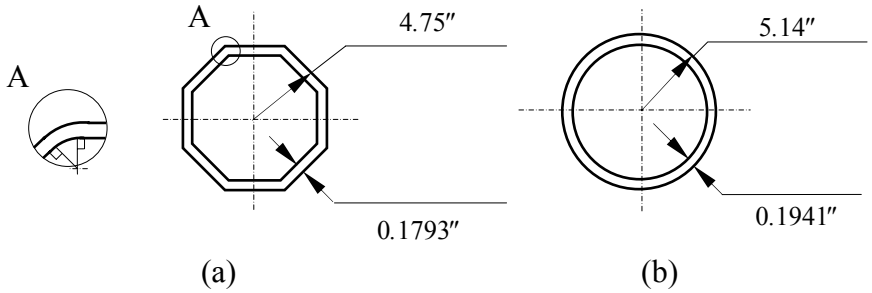

Figure 5.1 Cross-section of mast arm: (a) Octagonal, (b) Circular

5.1.2 Stress Distribution and Stress Concentration Factor

The finite element analysis indicates that the longitudinal stress in the direction of the mast arm centerline is always dominant under wind loads from any direction. The maximum stress occurs near the toe of welding at the corner of the octagonal section and at the uppermost point of the circular section. To see this clearly, the contour of the longitudinal stress caused by the galloping load for octagonal and circular section-arm is shown in Figure 5.2, and the stress distribution along the centerline of the arm is given in Figure 5.3. It can be seen that the longitudinal stress is the maximum at the toe of the weld and rapidly drops to its asymptotic value in the area away from the weld connection. The stress concentration factor, the ratio of stresses at weld toe on the mast arm and at any point far away from the weld toe, can be determined from Figure 5.3 to be 2.88 for the octagonal arm and 2.63 for the circular arm. The longitudinal stress distribution for the galloping loads at the weld toe around the arm is shown in Figure 5.4 in which one can see the stress amplitude increases significantly at each corner of the octagonal cross-section arm, and at the uppermost point of the circular cross-section arm. The stress distribution induced by natural wind gust or truck-induced gust follows the same curve as that induced by galloping load and the stress concentration factor are the same for the above-mentioned three types of forces.

5.2 Crack Initiation Life

A well-designed engineering structure may potentially fail under low amplitude cyclic loading in two stages: initiation and propagation of a crack. In general, the first stage lasts significantly longer than the second stage. The fatigue initiation life of the instrumented mast arm is predicted as follows.

The strain-life approach is used to predict the initiation life of the mast arms in the first stage. It required the use of the stress-strain and the strain-life relationships as described in Equation 5.1 and 5.2 (Bannantine *et al.*, 1990).

$$\frac{\Delta\varepsilon}{2} = \frac{\Delta\sigma}{2E} + \left(\frac{\Delta\sigma}{2K'}\right)^{1/n'} \tag{5.1}$$

$$\frac{\Delta\varepsilon}{2} = \frac{\sigma_f'}{E}(2N_f)^b + \varepsilon_f'(2N_f)^c \tag{5.2}$$

in which $\Delta\varepsilon$ and $\Delta\sigma$ respectively denote the cyclic strain and stress ranges on the mast arms, E is the modulus of elasticity of material used for the mast arm, and K' and n' represent the cyclic strength coefficient and the cyclic strain hardening exponent, respectively of the material. In Equation 5.2, N_f is the minimum number of cycles after which a crack initiates, and σ_f' and ε_f' are respectively the fatigue strength and ductility coefficients, and b and c are their corresponding exponents.

To determine the parameters in the above equations, ten flat-sheet specimens were made from the failed mast arm and tested on MTS810 machine according to the ASTM standard E606-92. The test results are presented in Figure 5.5. The parameters in Equation 5.1 and 5.2 are identified by curve fitting the plastic strain-stress and the strain-life model with the experimental data and they are listed in Table 5.1. The corresponding parameters of A-595A steel determined

using the monotonic stress-strain relation and other associated material properties are also listed in Table 5.1. The general agreement between the two sets of data gives assurance.

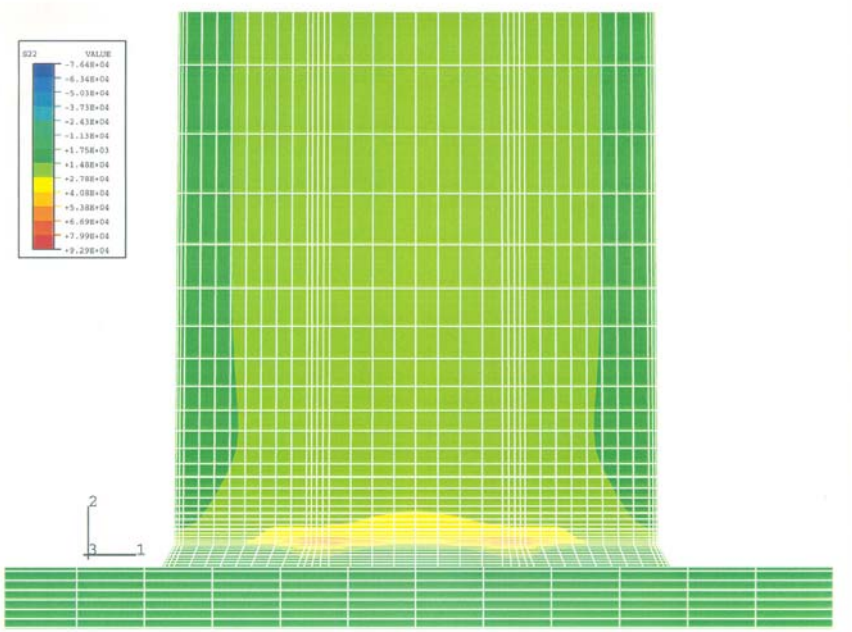

(a) Octagonal section

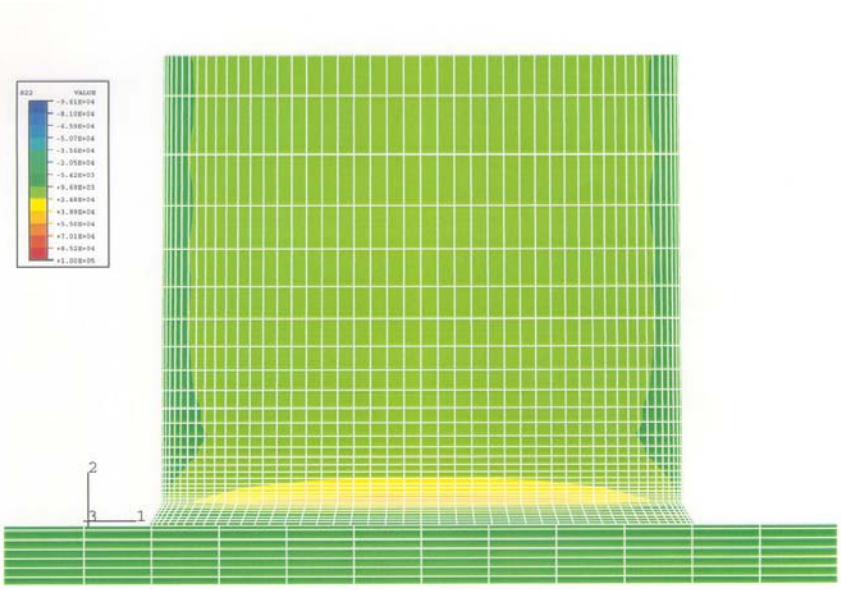

(b) Circular section

Figure 5.2 Stress contour around arm-post connection

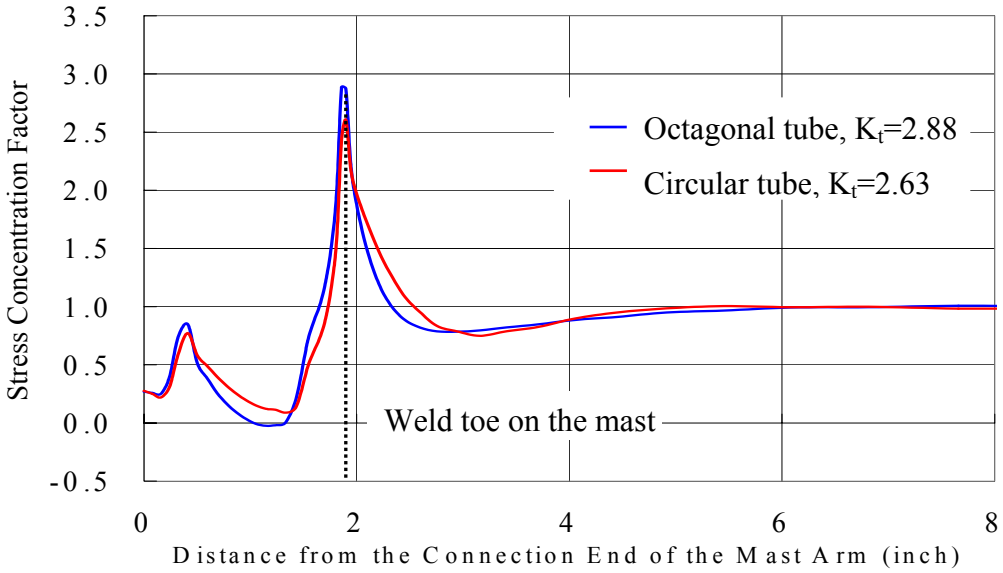

Figure 5.3 Stress distribution along the centerline of the arm

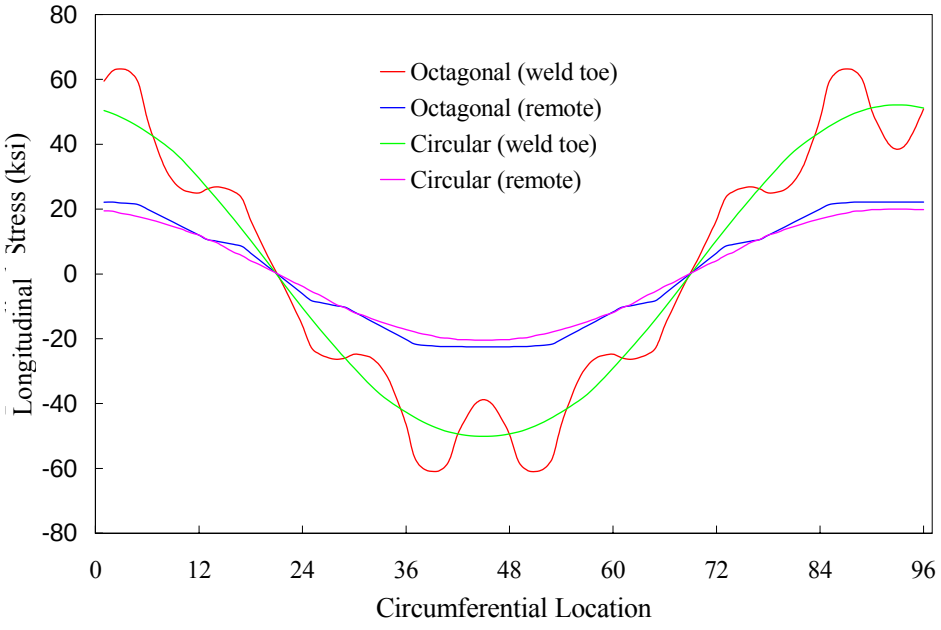

Figure 5.4 Stress distribution along the perimeter of mast arms

To determine the fatigue life under constant amplitude stress cycles, N_f, the maximum stress range $\Delta\sigma$ at the arm-post connection was first calculated using the Neuber's Rule as described in Equation 5.3 (Bannantine *et al.*, 1990). The normal stress range ΔS in Equation 5.3 is shown in the first column of Table 5.2 and Table 5.3, which is extrapolated from the strain measurement of gauge #3. The calculated results are listed in the second columns of Table 5.2 and 5.3, each representing the maximum stress at the arm-post connection. The fatigue life corresponding to each stress level is then determined from Equation 5.1 and 5.2 and included in the last column of the tables.

$$K_t^2 \frac{\Delta S}{2}\left[\frac{\Delta S}{2} + \left(\frac{\Delta S}{2K}\right)^{1/n'}\right] = \frac{\Delta\sigma}{2}\left[\frac{\Delta\sigma}{2E} + \left(\frac{\Delta\sigma}{2K'}\right)^{1/n'}\right] \tag{5.3}$$

The fatigue lives corresponding to various stress ranges are combined with the Miner's rule to determine the fatigue initiation life accounting for variable amplitude stress cycling (Bannantine *et al*., 1990). Based on this rule, both the Stadium & Forum and the Providence & Green Meadows arms are found fatigue adequate to survive natural wind gusts.

5.3 Effect of Weld Profile on the Stress Concentration

The Missouri Department of Transportation has recently introduced a so-called fatigue resistant weld profile with varying slopes. For this weld profile, the weld length on the mast arm is 1.83T, and that on the base plate is 1.57T, where T is the weld throat, i.e. the shortest distance between the root of the joint and the face of the weld. The maximum slope of the fatigue resistant weld is 30 degree. To understand the effects of weld profile on the stress concentration, four profiles for the octagonal mast arm are selected as shown in Figure 5.6(a). Profile (i) is the typical weld used in the current structure. Profile (ii) is a comparative weld, which possesses the same area as that of (i), but its slope on the mast arm is 45 degree. Profile (iii) is a fatigue-resistant weld with the weld throat equal to the thickness of the mast arm tube (0.1793 in). Profile (iv) is another fatigue-resistant weld. Its length on the mast arm is equal to that of Profile (i). Their effects on the stress concentration are presented in Figure 5.6(b). It can be observed that the actual weld yields the smallest concentration of stress with a factor of 2.88 at the weld toe even though its weld leg on the base plate is the shortest. This is mainly because the actual weld has the longest weld leg and the smallest slope on the mast arm wall. The stress concentration factor for the 45-degree weld is 3.01, although it has the same weld area as (i). The fatigue-resistant weld 1 has the largest stress concentration factor of 3.09, because its length on the mast arm is the shortest. Increasing the length of the fatigue-resistant weld to that of the actual weld, the stress concentration factor will be decreased to 2.96. Therefore, it is concluded that the stress concentration not only depends upon the slope of a weld profile but also depends on the weld length along the mast arm wall. The fatigue-resistant design could lessen the stress concentration if used to lengthen the weld leg on the arm wall.

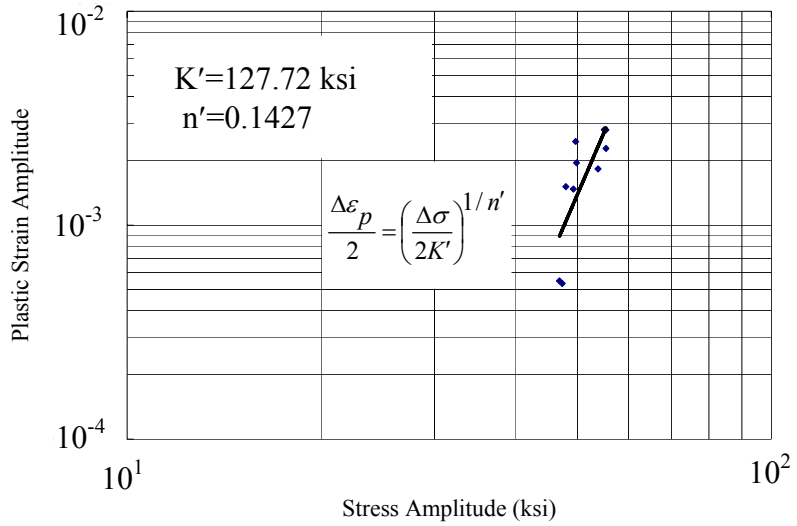

(a) Plastic strain and stress relation

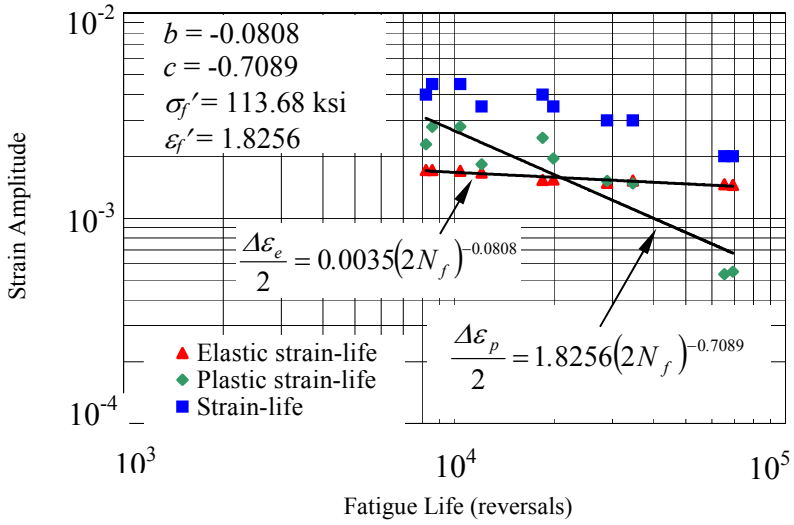

(b) Strain and fatigue life relation

Figure 5.5 Parameters in the crack initiation prediction model

Table 5.1 Parameters in the Stress-Strain and Strain-Life Models

Material	E (ksi)	K' (ksi)	n'	σ_f' (ksi)	ε_f'	b	c
Mast Arm Steel	32.28 x10^3	127.72	0.1427	113.68	1.8256	-0.0808	-0.7089
A-595A Steel	29.00 x10^3	115.07	0.1463	114.97	0.9943	-0.0878	-0.5~-0.7*

*Estimated based on experience

Table 5.2 Crack Initiation Life of the Mast Arm at Stadium & Forum Blvd.

Stress Range At Gauge #3 (ksi)	Stress Range At Arm-Post Connection (ksi)	Annual Number Of Loading Cycles	Minimum Number of Cycles Before Cracking
0.25	0.658	1.404×10^7	*
0.75	1.973	5.412×10^6	*
1.50	3.945	2.559×10^6	*
2.50	6.575	8.401×10^5	*
3.50	9.205	2.445×10^5	*
4.50	11.84	1.086×10^5	*
5.50	14.47	5.767×10^4	*
6.50	17.10	4.335×10^4	*
7.50	19.73	1.295×10^4	*
8.50	22.36	8.216×10^3	*
9.50	24.99	4.773×10^3	*
11.0	28.93	5.378×10^3	*
13.0	34.19	2.133×10^3	*
15.0	39.45	7.807×10^2	5.15×10^9
17.0	44.71	6.934×10^2	1.08×10^9
19.0	49.97	5.825×10^1	2.64×10^8
21.0	55.23	8.159×10^1	7.32×10^7
23.0	60.49	4.663×10^1	2.24×10^7

* Number of Cycles > 10^{10}

Table 5.3 Crack Initiation Life of the Mast Arm at Province & Green Meadows Rd.

Stress Range At Gauge #3 (ksi)	Stress Range At Arm-Post Connection (ksi)	Annual Number Of Loading Cycles	Minimum Number of Cycles Before Cracking
0.10	0.288	1.742×10^7	*
0.30	0.864	5.515×10^6	*
0.55	1.584	3.401×10^6	*
0.85	2.448	9.522×10^5	*
1.25	3.600	4.648×10^5	*
1.75	5.040	1.269×10^5	*
2.25	6.480	2.814×10^4	*
2.75	7.920	1.289×10^4	*
3.50	10.08	6.387×10^3	*
4.50	12.96	1.207×10^3	*
5.50	15.84	2.943×10^2	*
6.50	18.72	3.044×10^1	*
7.50	21.60	2.029×10^1	*

* Number of Cycles > 10^{10}

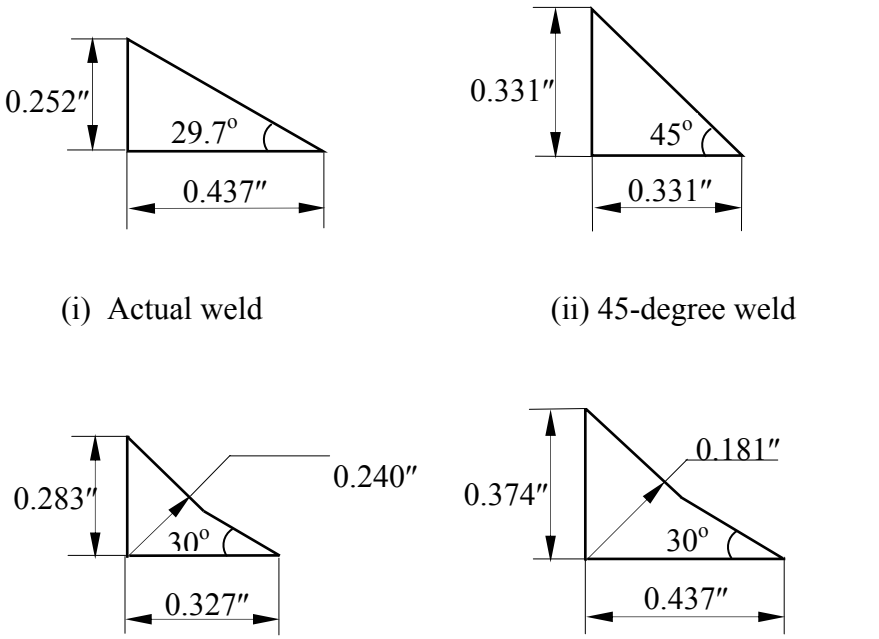

(i) Actual weld (ii) 45-degree weld

(iii) Fatigue-resistant weld 1 (iv) Fatigue-resistant weld 2

(a) Weld profiles

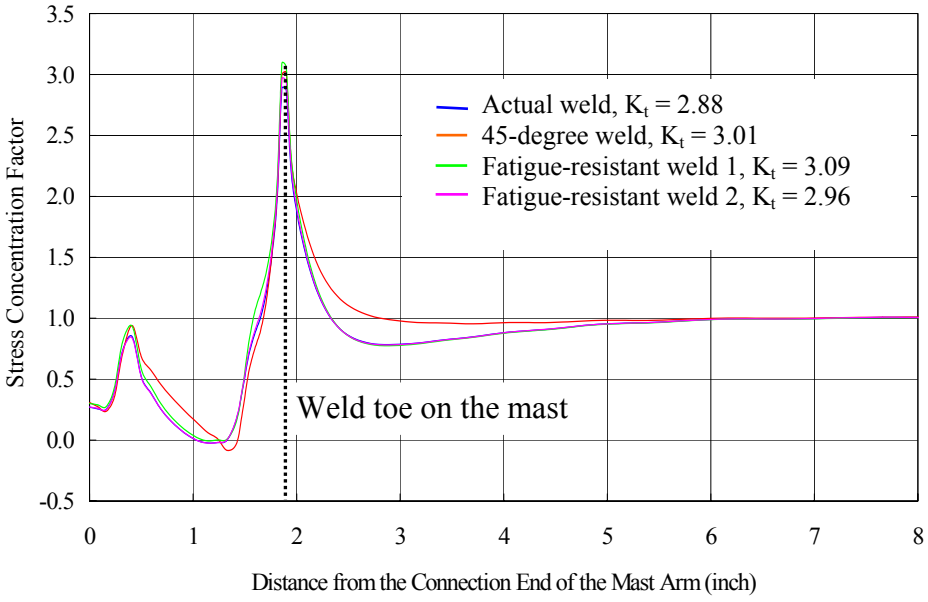

(b) Stress concentration factors

Figure 5.6 Stress concentration factors for various weld profiles

5.4 Conclusion for Stress Analysis and Crack Initiation Life

From the above analysis, the longitudinal stress along the axis of the mast arm is dominant for all the kinds of the fatigue-related forces. The stress reaches its peak value near the weld toe on the mast arm. Of the two types of the mast arm sections, the stress concentration factor at the weld toe for the octagonal mast arm is larger than that for the circular mast arm. Due to stress concentration, circular cross-section mast arms often have slightly better fatigue performance. The slope and the length of the weld on the mast arm affect the stress concentration. The fatigue-resistant-design weld is beneficial as long as the length of the weld on the mast arm is long enough. Both the Stadium & Forum and the Providence & Green Meadows arms are found fatigue adequate to survive natural wind gusts.

5.5 Remaining Life Models

In response to the need to assess the resistance to failure of structures that contain initial defects or discontinuities that develop fatigue cracks, remaining life models were established as follows. Assume there is a small surface crack near the toe of weld profile on the mast arm. The mast arms can still support the external loads until the defect propagates around the cross section of the arms. The crack growth rate is related to the range of stress intensity factor, ΔK, by the following Paris equation (Bannantine *et al.*, 1990):

$$\frac{da}{dN} = C(\Delta K)^m \tag{5.4}$$

in which a is the crack length, N is the number of stress cycle applied to the structure, and C and m are two material constants. To determine these two constants, several compact tension specimens were made from the failed octagonal mast arm and tested in the MTS810 system according to ASTM standard E 647 - 95a. The test specimen and setup is shown in Figure 5.7(a). The material constants can be estimated as $C = 2.36 \times 10^{-10}$ in the units of a as inch and K as ksi$\sqrt{in}$ and m=3.11 from the test data shown in Figure 5.7(b).

Consider a thumbnail surface crack shown in Figure 5.8. The initial crack length is supposed as 0.05 inch, which is the maximum length of surface defects NDT can defect. For the surface crack, suppose *a/2c* equal to 0.1. For the crack shown in Figure 5.8, the stress intensity factor K is a function of stress at the arm-post connection and the crack size, etc. The following equation can be used to calculate K (Bannatine *et al*., 1990).

$$K_I = 1.12\sigma\sqrt{\pi\frac{a}{Q}}M_k \tag{5.5}$$

where $M_k = 1.0$ for $a < 0.5t$, and $M_k = 1.0 + 1.2\left(\frac{a}{t} - 0.5\right)$ for $a > 0.5t$. Q is a function of $a/2c$ and σ/σ_{ys}.

(a) Test specimen and setup

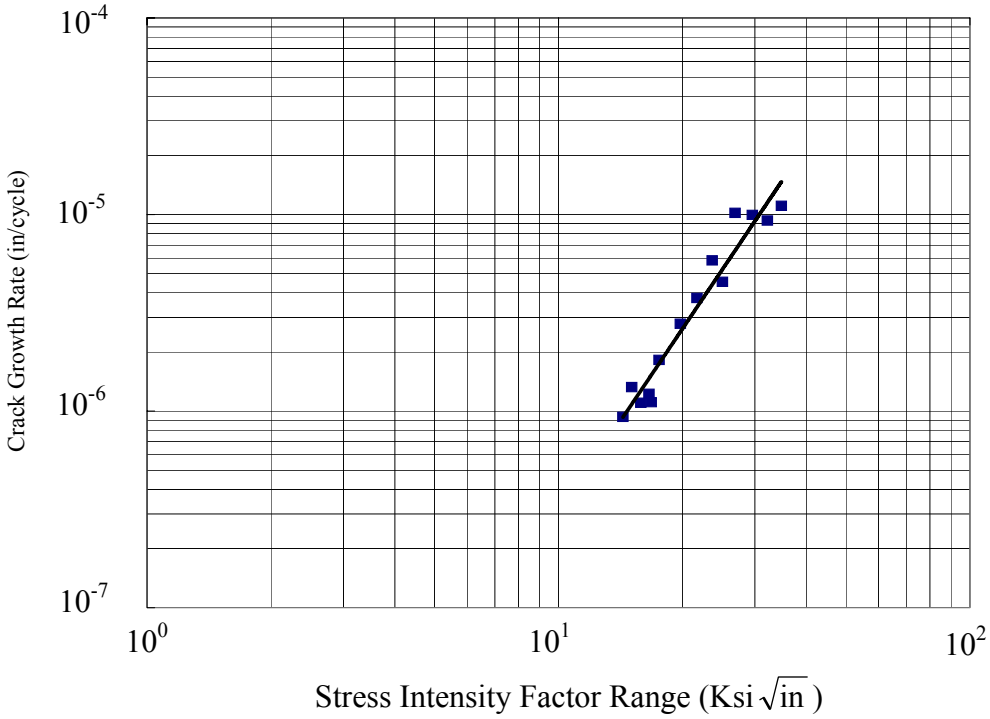

(b) Crack growth rate vs. stress intensity factor range

Figure 5.7 Determination of constants in the crack growth rate model

A numerical approach with the crack length increment of 0.0068 inch was used to predict the crack propagation life using Equation 5.4. The Root-Mean-Square model was used to predict the fatigue propagation life under variable amplitude loading such as natural wind gust. This model uses the root-mean-square stress intensity factor to represent different stress level.

$$\Delta K_{rms} = \sqrt{\sum_{i=1}^{n} \frac{\Delta K_i^{\,2}}{n}} \tag{5.6}$$

where n is the number of cycles, and ΔK_i is the stress intensity range associated with i^{th} cycle.

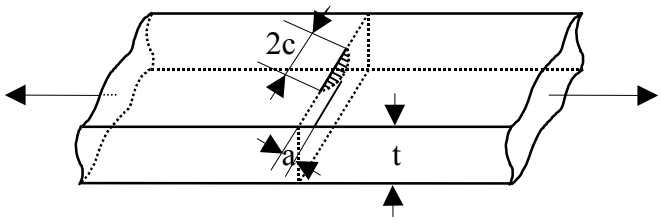

Figure 5.8 The part through thumbnail crack

For each increment of crack length, compute ΔK_i for different stress level, and then use Equation 5.5 to get ΔK_{rms}. Use $\frac{\Delta a}{\Delta N} = C(\Delta K_{rms})^m$ to get ΔN_i. The total crack propagation life in cycles was obtained by summing ΔN_i. Figure 5.9 and 5.10 show the crack propagation life for different initial crack length.

In the above calculation of crack initiation and propagation life, the following assumptions are made. First, the weld is a perfect connection, i.e., there is no inclusion, no discontinuity and no lack-of-penetration. These assumptions induce a very long initiation life. Second, use the maximum local stress to calculate the crack propagation life. This stress caused the result to be too conservative.

For welded structures, the above-mentioned flaws (such as inclusions, discontinuity, lack of penetration and undercut) are likely to be present; it is reasonable to assume that the entire fatigue life of the structure to consist of crack propagation phase. By comparing the predicted life with that determined experimentally in Section 2.3, a modified stress concentration factor is calculated for each cross section (octagonal and circular) of the mast arm. These modified stress concentration factors are 1.25 for octagonal section and 2.03 for circular section. Here, the analytical model predictions and the experimental test fatigue life data correspond to constant amplitude loading case. Using these stress concentration factors that are calibrated using constant amplitude fatigue data, the crack propagation life (remaining life) of the mast arm subjected to natural wind gusts (variable amplitude loading) is calculated. The remaining life predictions for the mast arm at Providence & Green Meadows and at Stadium & Forum are given in Figures 5.11-5.14.

For the remaining life model corresponding to 1.6 million cycle fatigue life for the lab test, a 0.05-inch crack will lead to the fracture of the Stadium & Forum mast arm after 40.2 years of service and the fracture of the Province & Green Meadows after 928 years of service. Even a 0.104-inch crack will not yield collapse of the first arm for 9.3 years and the second arm for 214 years. For the remaining life model corresponding to 0.4 millions cycle fatigue life for the lab

test, a 0.05-inch crack will lead to the fracture of the Stadium & Forum mast arm after 8.9 years of service and the fracture of the Province & Green Meadows after 206 years of service. A 0.104-inch crack will not yield collapse of the first arm for 2.1 years and the second arm for 47.4 years. Thus, it is concluded that the first arm is likely vulnerable to the development of any finite size of crack because the stress level is relatively high (the mast arm is longer) while the second arm is not unless a visible crack is developed. It also shows that the higher modified stress concentration factor (due to poor weld quality and the location of defects) will decrease the structural fatigue life dramatically.

5.6 Summary

Based on the above analysis, the following conclusions can be made:

1. The stress concentration occurs at the weld toe on the mast arm at the mast-post connection. For the actual welded structures, the maximum stress occurs at the uppermost point of the circular section with a concentration factor of approximately 2.63, and at the upper corner of the octagonal section with a concentration factor of approximately 2.88. Because of stress concentration, use of circular cross sections often improves slightly the fatigue performance of mast arms. The stress concentration factor also depends on the slope and the length of the weld toe on the mast arm. The fatigue resistant design may be helpful in decreasing the stress concentration factor as long as the weld leg on the mast arm is long enough.
2. For a perfect connection, both of the mast arms investigated here will not initiate a crack over the life span of their service under natural wind gusts.
3. Due to the initial weld defects or discontinuities or lack-of-penetration, the remaining fatigue life can be considered equal to the crack propagation life. With the stress concentration factor correlated with the fatigue tests in Section 2.3, the remaining fatigue life for the mast arm was predicted. The Stadium & Forum mast arm is likely vulnerable to the development of any finite size crack because the stress level is relatively high (the mast arm is longer) while the Providence & Green Meadows mast arm is not unless a visible crack is developed. The magnitude of the modified stress concentration factor due to the quality of weldment also affects the remaining fatigue life.

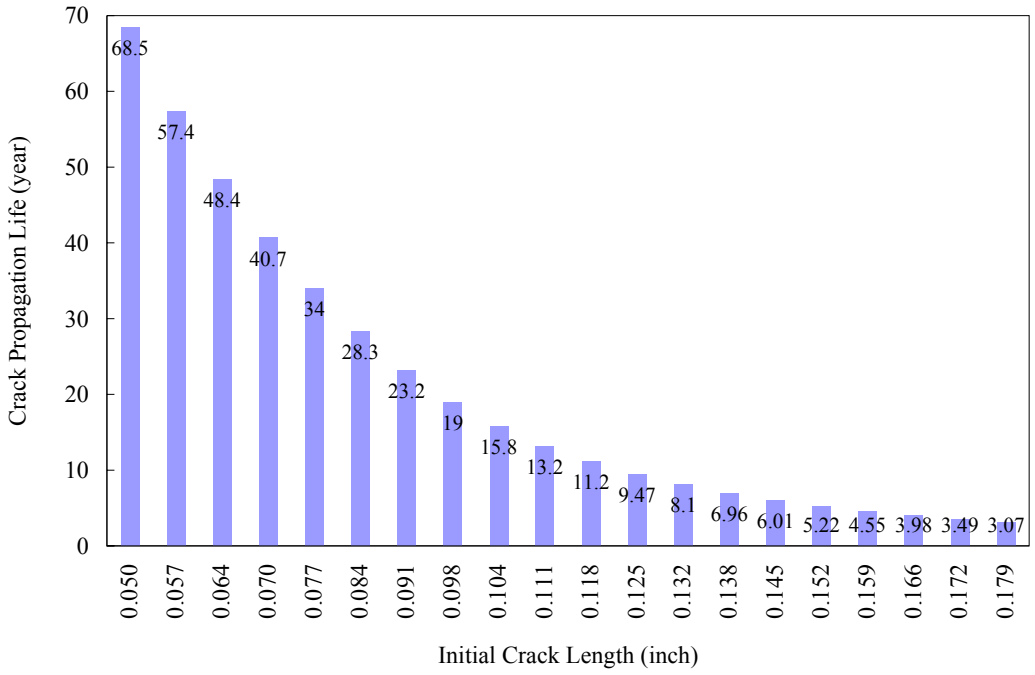

Figure 5.9 Crack propagation life for the mast arm at Providence & Green Meadows

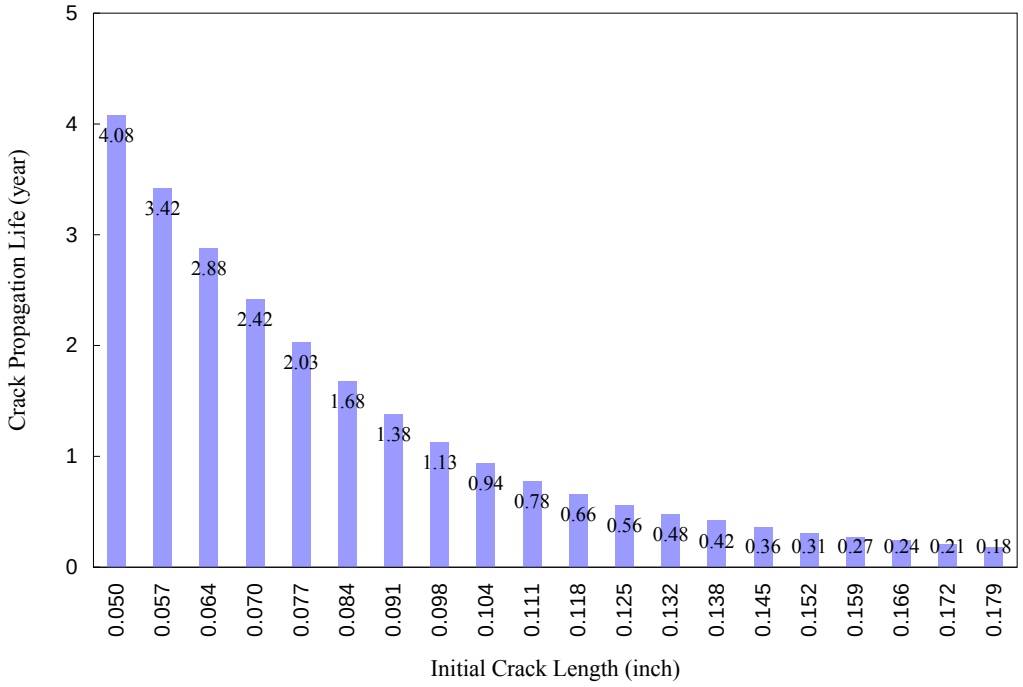

Figure 5.10 Crack propagation life for the mast arm at Stadium & Forum

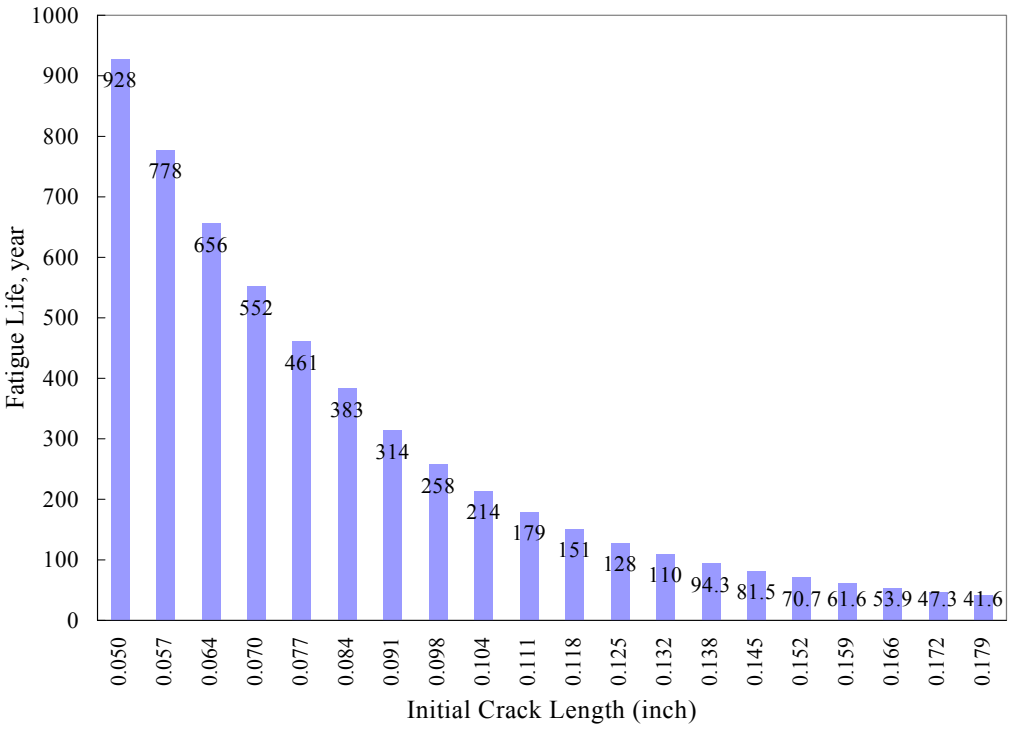

Figure 5.11 Remaining fatigue life for the mast arm at Providence & Green Meadows (correlated with 1.8 million cycles fatigue life for the lab test)

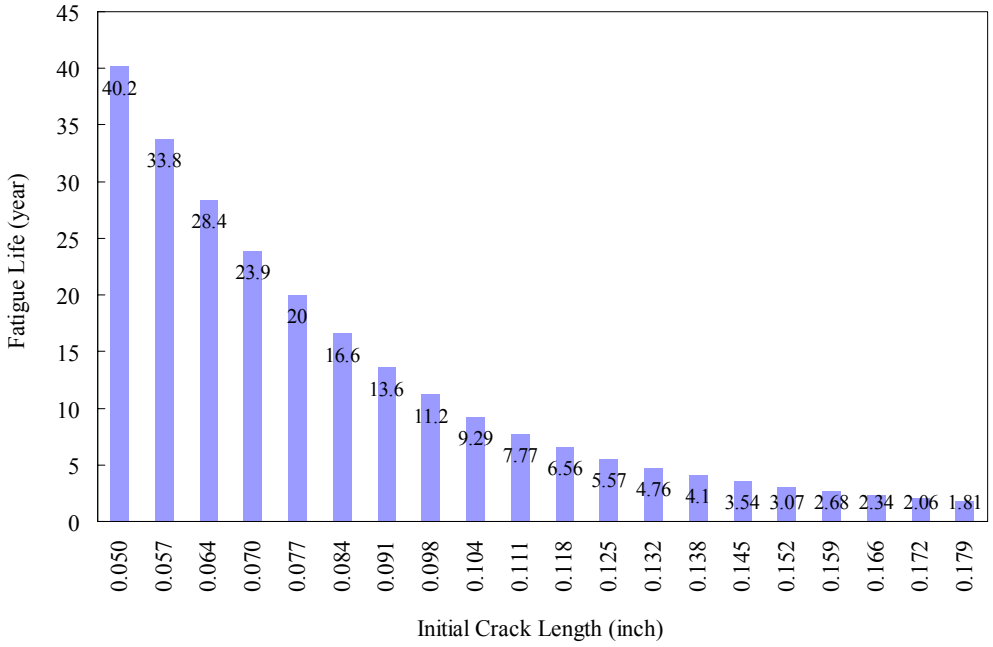

Figure 5.12 Remaining fatigue life for the mast arm at Stadium & Forum (correlated with 1.8 million cycles fatigue life for the lab test)

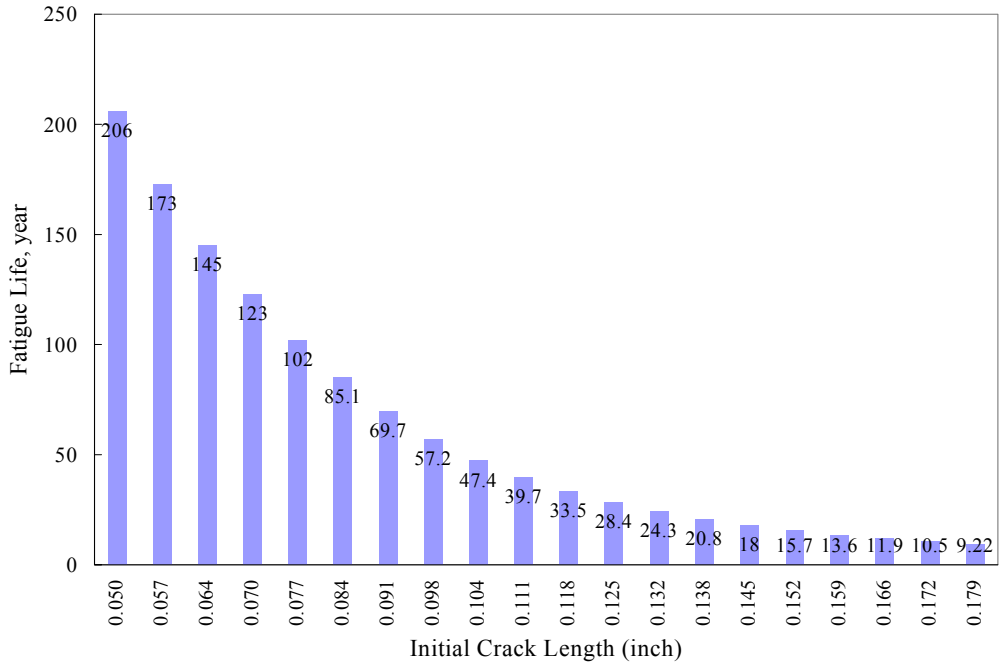

Figure 5.13 Remaining fatigue life for the mast arm at Providence & Green Meadows (correlated with 0.4 million cycles fatigue life for the lab test)

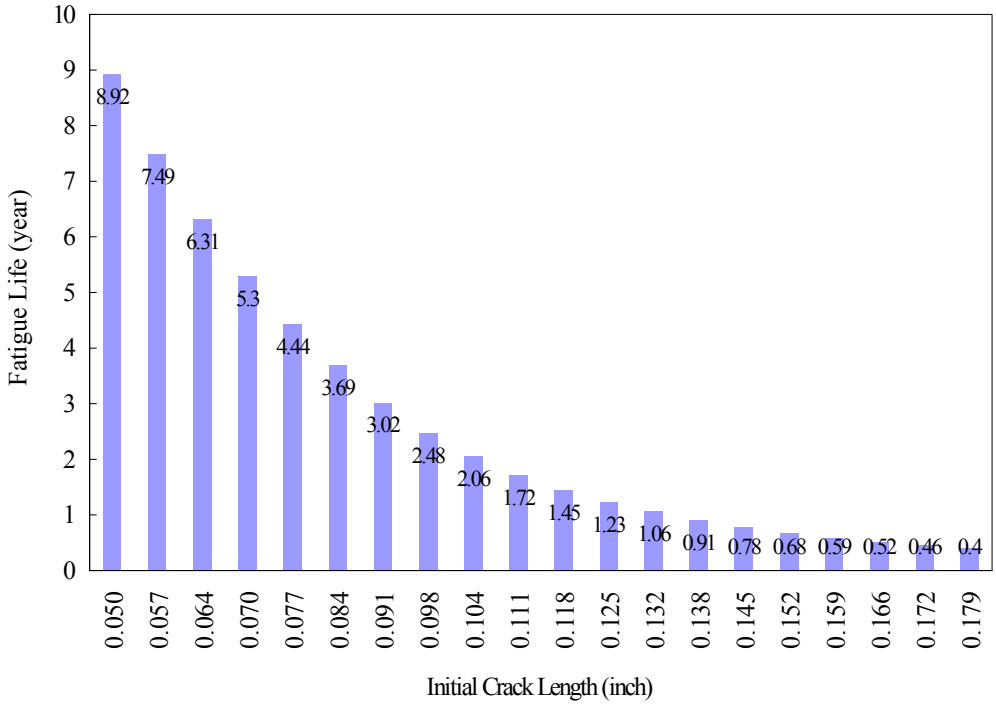

Figure 5.14 Remaining fatigue life for the mast arm at Stadium & Forum (correlated with 0.4 million cycles fatigue life for the lab test)

6. CONCLUSIONS AND RECOMMENDATIONS

6.1 Results of Individual Project Components

Based on the fatigue tests of five mast arms in the laboratory, metallurgical failure analysis of two out of the five laboratory-tested arms and a mast arm failed in field condition, and extensive numerical simulations of loading spectrum and remaining fatigue life, the following conclusions can be drawn:

1. Failure of the signal mast arm initiated by fatigue cracking on the outside weld at the weld toe. Crack initiation was enhanced by the presence of weld undercutting, creating a sharp geometrical stress concentration. The location of the undercutting at the heat affected zone of the base material, where the base material is softest, further contributed to early fatigue failure.
2. The welds are of poor quality and exhibited lack of penetration and lack of fusion. However, this lack of penetration and lack of fusion did not contribute directly to the premature failure of the signal mast arms.
3. The weldments of the two mast arms tested to failure in the laboratory and analyzed have sharp features very similar to those examined for the in-service failed arm. Their failure mechanism is thus the same, even though one of the arms tested to failure in laboratory was designed with the new weld profile.
4. Laboratory tests indicated that two out of the three mast arms manufactured by Valmont company performed satisfactorily while both arms manufactured by JEM, Inc. and Union Metals, respectively, failed prematurely. Test results also verified that the new weld profile does not necessarily delay the initiation of cracking in mast arms.
5. The forensic investigation on the two arms tested to failure in the laboratory indicated that both have poor weld quality and fractured due to initiation of the crack at the weld toe though the laboratory tests resulted in quite different fatigue strengths. The difference in fatigue strength (number of cycles) of the two arms is likely due to other factors that were not taken into account in the forensic investigation, such as residual stress on the base metals.
6. The new *American Association of State Highway and Transportation Officials* (AASHTO) Specifications (1999) required significantly higher loading on traffic signal supported structures for design. According to the Specifications, the existing arms examined fatigue inadequate. The dimensions of the two in-service mast arms instrumented for this research project must increase substantially to meet the standard requirements.
7. Both the wind speed and the ratio between stress and the square of wind speed follow the logarithmic normal distribution. Since the ratio is insensitive to the wind speed, its distribution can be used for both weak and strong wind gusts.
8. The average stress in the signal arm structure at Forum & Stadium Blvd. is significantly larger than that at Providence & Green Meadows Rd. due to its longer

span. The intensity of vertical vibration caused by natural wind gusts is less than 1/3 of that of horizontal vibration.

9. The stress concentration occurs at the weld toe of the arm-post connection. The maximum stress occurs at the uppermost point of the circular section with a concentration factor of approximately 2.63 and at the corner of the octagonal section with a concentration factor of approximately 2.88. The stress concentration depends upon the length of weld leg along the mast arm wall. The fatigue resistant design proposed by the Missouri Department of Transportation may, therefore, be helpful in slowing down the propagation of crack initiated at the weld toe.
10. Both instrumented signal structures will not crack during the life span of their service. However, the mast arm at the Stadium & Forum Blvd. is likely to be vulnerable to the development of a crack, but the mast arm at the Providence & Green Meadows Rd. is not, unless a visible crack has been developed.
11. Although the field instrumentation on two mast arms did not pick up severe vibration associated with the wind-induced galloping effect, the evaluation based on the currently-available theoretical model indicated that the mast arm with octagonal cross section has a high potential to galloping during a strong wind event.

6.2 Description of Recommendations

Failure of mast arm-post connections can be reduced or eliminated either by increasing their fatigue strength or reducing the maximum cyclic stress. A well-prepared weld connection can improve the strength to resist cyclic stress while mechanical approaches can be used to reduce the stress on critical connections. Based on the extensive investigations in this project, the following recommendations are made for the new design and retrofitting of existing structures. They are presented in separate sections.

6.2.1 Existing Mast Arms

1. The cyclic stress on a weld joint can be reduced with addition of several stiffeners between a mast arm and its base plate. These stiffeners can be evenly distributed around the perimeter of the mast arm for increased cross section. The potential disadvantage of this method is that it is difficult to maintain high quality welds in field conditions.
2. A measurable improvement in the fatigue life could be obtained by shot peening the weld surface. This effort would impart a compressive residual stress at the surface, and may smooth out any undercutting.
3. Although the maximum stress of the mast arms instrumented in this study is relatively small, potential for galloping of the mast arms exists. Therefore, a quick screening analysis following the procedure described in Section 4.3 is necessary for existing arms and the emerging technology such as damping mechanism can be applied to suppress the excessive vibration of inadequate arms.

6.2.2 New Mast Arms

1. The weld joint can be improved by the use of a bevel weld preparation. The bevel should be approximately equal to the signal mast arm wall thickness. This will improve the penetration and fusion. It will also improve the weld bead profile. The joint preparation should be included in the standard drawings.
2. The welding practice of the fabricator of the signal mast arms should be investigated. The weld must be made such that it contains no undercutting. Engineering drawings and inspection criteria must be modified to state that undercutting at the toe of the weld bead is not permitted.
3. The fabricator of the mast arms should undergo a regularly scheduled audit of the process to insure that proper welding parameters (such as current, voltage, weld electrode type, etc.) be in place and maintained. In addition, the audit should include that the weld technicians are properly trained and certified in order to insure the quality of the welds produced.
4. Inspection of the weldments to determine whether or not undercutting is present is of paramount importance in the production of sound mast arms. Since the most important parameter in fatigue life is crack initiation, it must be insured that undercutting or the production of a geometrical stress concentration at the toe of the weld does not occur. If such a feature is present, the mast arm must be repaired or scrapped.

6.3 Future Work

While most recommendations will certainly lead to the positive improvement of the weld connection performance, other retrofitting techniques need to be developed and verified experimentally. Future research will be directed to the laboratory demonstration of the efficiency of a bevel weld preparation and the performance of a weld connection strengthened with stiffeners. Additionally, fatigue failure is related to cyclic stress caused by natural wind gusts and truck passages. The emerging damping technology such as tuned mass dampers studied by the Texas Department of Transportation can be very effective in suppressing the vibration of mast arms. However, the actual effectiveness of such techniques for mast arm applications in Missouri is yet to be explored due to different structural details and wind environments.

Since undercutting in the arm-post weld connection is critically important in crack initiation, it is necessary to evaluate AWS specifications for the specific applications in Missouri mast arms. The issue of allowable undercutting needs to be further studied for the weld detail used in mast arms.

7. IMPLEMENTATION

Research will work with Traffic to consider recommendations for existing arms and with Bridge to consider recommendations for new mast arms. Since the initiation of the project, the Bridge Division at MoDOT requires that mast arm fabricators be AISC certified. The AISC Certification provides a third party opinion of the fabricators quality control and quality assurance.

8. BIBLIOGRAPHY

Alderson, J. "Fatigue Study of Cantilever Traffic Signal Mast Arms." Masters Thesis, University of Missouri-Columbia, Columbia, MO, Dec. 1999, 120pp.

American Association of State Highway and Transportation Officials (AASHTO). Standard Specifications for Structural Supports for Highway Signs, Luminaires and Traffic Signals, 1994.

American Association of State Highway and Transportation Officials (AASHTO). Standard Specifications for Structural Supports for Highway Signs, Luminaires and Traffic Signals, Third Draft, 1999.

Bannantine, J.A., J.J. Comer, and J.L. Handrock. Fundamental of Metal Fatigue Analysis. Prentice Hall, 1990.

Bennett, R.E. MoDOT Interoffice Memo to L.J. Grinther, May 27, 1997.

Chen, G.D., J.N. Wu, J. Q. Yu, L.R. Dharani, and M.G. Barker. "Fatigue Assessment of Traffic Signal Mast Arms Based on Field Test Data under Natural Wind Gusts." Proc. 2001 Transportation Research Board Meeting, Washington, D.C., January 7-11, 2001 (CD-Rom).

Creamer, B.M., K.H. Frank, and R.E. Klinger. Fatigue Loading of Cantilever Sign Structures from Truck Wind Gusts. Research Report 209-1F, University of Texas at Austin, 1979.

Edmund Ung. Changeable Message Sign District 8. Instrumentation activity Report, California Department of Transportation, 1996.

Gray, B., P. Wang, H.R. Hamilton, and J.A. Puckett. "Traffic Signal Structure Research at the University of Wyoming." Proc. 1999 Structures Congress, ASCE, New Orleans, LA, April 18-21, 1999, pp. 1107-1110.

Hillner, L. MoDOT Interoffice Memo to R. Bennett, May 13, 1997.

Kaczinski, M.R., R.J. Dexter, and J.P. Van Dien. Fatigue-Resistant Design of Cantilevered Signal, Sign and Light Supports, Technical Report 412, Transportation Research Board, National Academic Press.

Porter, P. MoDOT Interoffice Memo to J. Jackson, July 08, 1996.

Simiu, E. and R. H. Scanlan. Wind Effects on Structures. John Wiley & Sons, Inc., Third Edition, 1996.

9. APPENDIX A: ANNUAL PERCENTAGE OF WIND EVENTS AT COLUMBIA

	WIND DIRECTION																	
SPEED (m/sec)	N	NNE	NE	ENE	E	ESE	SE	SSE	S	SSW	SW	WSW	W	WNW	NW	NNW	CALM	TOTAL
CALM	.0	.0	.0	.0	.0	.0	.0	.0	.0	.0	.0	.0	.0	.0	.0	.0	2.3	2.3
1	.0	.0	.0	.0	.0	.0	.0	.0	.0	.0	.0	.0	.0	.0	.0	.0	.0	.2
2	.7	.4	.5	.6	1.1	.6	.8	.8	1.9	.4	.5	.5	.7	.6	.5	.4	.0	11.2
3	1.3	.7	1.1	1.2	1.9	1.6	2.2	1.7	3.4	.8	.9	.9	1.3	1.3	.9	.7	.0	22.0
4	1.2	.8	1.0	1.0	1.2	1.8	2.3	2.0	3.5	1.2	1.3	1.0	1.1	1.5	.9	.8	.0	22.5
5	1.0	.6	.6	.5	.7	1.2	1.4	1.3	2.3	.9	.9	.6	.8	1.2	.9	.7	.0	15.4
6	.8	.3	.3	.2	.4	.5	.7	.7	1.5	.7	.6	.4	.6	.8	.9	.6	.0	10.0
7	.6	.2	.2	.1	.2	.4	.5	.5	1.1	.5	.5	.3	.5	.8	.8	.4	.0	7.6
8	.4	.1	.1	.1	.1	.2	.3	.3	.7	.3	.3	.2	.3	.6	.5	.3	.0	4.8
9	.2	.0	.0	.0	.0	.0	.1	.2	.3	.2	.1	.2	.2	.4	.3	.1	.0	2.3
10	.1	.0	.0	.0	.0	.0	.0	.1	.1	.1	.1	.1	.1	.1	.2	.1	.0	1.0
11	0	.0	.0	.0	.0	.0	.0	.0	.0	.0	.0	.0	.0	.1	.1	.0	.0	.3
12	.0	.0	.0	.0	.0	.0	.0	.0	.0	.0	.0	.0	.0	.0	.0	.0	.0	.2
13	.0	.0	.0	.0	.0	.0	.0	.0	.0	.0	.0	.0	.0	.0	.0	.0	.0	.1
14	.0	.0	.0	.0	.0	.0	.0	.0	.0	.0	.0	.0	.0	.0	.0	.0	.0	.0
15	.0	.0	.0	.0	.0	.0	.0	.0	.0	.0	.0	.0	.0	.0	.0	.0	.0	.0
16	.0	.0	.0	.0	.0	.0	.0	.0	.0	.0	.0	.0	.0	.0	.0	.0	.0	.0
17	.0	.0	.0	.0	.0	.0	.0	.0	.0	.0	.0	.0	.0	.0	.0	.0	.0	.0
18	.0	.0	.0	.0	.0	.0	.0	.0	.0	.0	.0	.0	.0	.0	.0	.0	.0	.0
19	.0	.0	.0	.0	.0	.0	.0	.0	.0	.0	.0	.0	.0	.0	.0	.0	.0	.0
20	.0	.0	.0	.0	.0	.0	.0	.0	.0	.0	.0	.0	.0	.0	.0	.0	.0	.0
21-25	.0	.0	.0	.0	.0	.0	.0	.0	.0	.0	.0	.0	.0	.0	.0	.0	.0	.0
26-30	.0	.0	.0	.0	.0	.0	.0	.0	.0	.0	.0	.0	.0	.0	.0	.0	.0	.0
31-35	.0	.0	.0	.0	.0	.0	.0	.0	.0	.0	.0	.0	.0	.0	.0	.0	.0	.0